Inhibitory signaling blocks activating receptor clustering and induces cytoskeletal retraction in natural killer cells

Thushara P. Abeyweera, Ernesto Merino, and Morgan Huse

Immunology Program, Memorial Sloan-Kettering Cancer Center, New York, NY 10065

Natural killer (NK) lymphocytes use a variety of activating receptors to recognize and kill infected or tumorigenic cells during an innate immune response. To prevent targeting healthy tissue, NK cells also express numerous inhibitory receptors that signal through immunotyrosine-based inhibitory motifs (ITIMs). Precisely how signals from competing activating and inhibitory receptors are integrated and resolved is not understood. To investigate how ITIM receptor signaling impinges on activating pathways, we developed a photochemical approach for stimulating the inhibitory receptor KIR2DL2 during ongoing NK cell–activating responses in high-resolution imaging experiments. Photostimulation of KIR2DL2 induces the rapid formation of inhibitory receptor microclusters in the plasma membrane and the simultaneous suppression of microclusters containing activating receptors. This is followed by the collapse of the peripheral actin cytoskeleton and retraction of the NK cell from the source of inhibitory stimulation. These results suggest a cell biological basis for ITIM receptor signaling and establish an experimental framework for analyzing it.

Introduction

Natural killer (NK) lymphocytes play a crucial role in antiviral and anticancer responses by killing infected or tumorigenic target cells and also by secreting inflammatory cytokines. They are activated by a diverse set of transmembrane receptors that recognize cell surface proteins characteristic of infected or transformed tissue (Lanier, 2005). Ligand binding triggers the elevation of intracellular calcium (Ca^{2+}), the up-regulation of integrin-mediated adhesion, and cytoskeletal reorganization leading to the formation of a radially symmetric cell–cell contact called the cytolytic synapse (Burshtyn et al., 2000; Orange et al., 2003; Barber et al., 2004; Bryceson et al., 2005; Stinchcombe and Griffiths, 2007). Soluble cytotoxic agents, such as perforin and granzyme, are then secreted by the NK cell into the synapse to kill the target (Stinchcombe and Griffiths, 2007).

Activating NK receptors are opposed by a group of inhibitory receptors that contain a cytoplasmic-signaling motif known as an immunotyrosine-based inhibitory motif (ITIM). Although ITIM receptors regulate multiple cell types, they are particularly important for the control of lymphocyte activity and the prevention of autoimmunity (Long, 2008). In NK cells, they block the cytolysis of normal healthy tissue by recognizing class I major histocompatibility complex (MHC), which is expressed on the surface of most cell types and serves as a marker for "self" (Lanier, 2005; Long, 2008). MHC binding induces ITIM phosphorylation and the subsequent recruitment of the tyrosine phosphatases SHP-1 and SHP-2 (Burshtyn et al., 1996; Olcese et al., 1996; Bruhns et al., 1999), which dephosphorylate signaling molecules required for activating responses (Binstadt et al., 1998; Stebbins et al., 2003).

Studies suggest that ITIM signaling in NK cells disrupts activating pathways at a level close to the activating receptor itself (Kaufman et al., 1995; Valiante et al., 1996; Guerra et al., 2002; Krzewski et al., 2006; Masilamani et al., 2006). Precisely how inhibitory signals interface with their activating counterparts within a cell–cell contact, however, is not understood. In T cells and B cells, activated antigen receptors signal from plasma

T.P. Abeyweera and E. Merino contributed equally to this paper.

Correspondence to M. Huse: husem@mskcc.org

Abbreviations used in this paper: DMNB, dimethoxy-nitrobenzyl; Fmoc, 9-fluorenylmethoxycarbonyl; HLA, human leukocyte antigen; ICAM, intercellular adhesion molecule; ITIM, immunotyrosine-based inhibitory motif; KIR, killer Ig receptor; MHC, major histocompatibility complex; MSCV, murine stem cell virus; NK, natural killer; SA, streptavidin; TIRF, total internal reflection fluorescence.

The Rockefeller University Press $30.00
J. Cell Biol. Vol. 192 No. 4 675–690
www.jcb.org/cgi/doi/10.1083/jcb.201009135

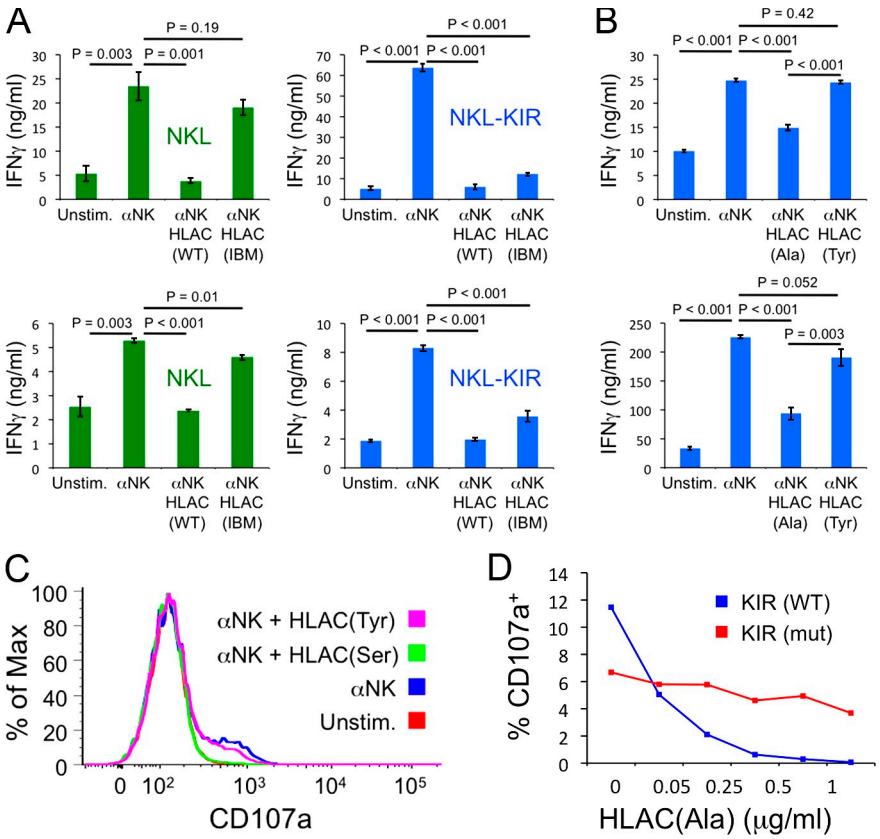

Figure 1. **KIR2DL2 signaling blocks activating responses.** (A) Control NKL cells (left) and NKL cells expressing KIR2DL2 (right) were stimulated with α-NK and either wild-type (WT) HLA-Cw3 or HLA-Cw3 containing the ILT2-binding mutation (IBM) as indicated. Both HLA-Cw3 proteins contained the importin-α peptide with p8 Ala. IFN-γ secretion was quantified by ELISA. Two independent experiments are shown for each cell type. Although maximal IFN-γ secretion varied from day to day, the relative differences in cytokine production between different stimulus conditions were consistent. All other figures presented in this paper used HLA-Cw3 containing the ILT2-binding mutation. (B–D) NKL cells expressing wild-type KIR2DL2 (B–D) or KIR2DL2(mut) (D) were added to plastic wells containing immobilized α-NK and the indicated HLA-Cw3 proteins. (B) IFN-γ secretion from NKL cells expressing KIR2DL2, measured by ELISA. Two independent experiments are shown. (C) Representative degranulation responses measured by surface expression of CD107a. Unstim., unstimulated. As with IFN-γ secretion, maximal degranulation responses were quite variable. However, the relative differences between stimulus conditions were consistent. (D) Dose–response curves showing induced degranulation from NKL cells expressing either wild-type KIR2DL2 or KIR2DL2(mut) (both Tyr 302 and Tyr 332 mutated to Phe) as a function of the concentration of HLA-Cw3(Ala) used during protein immobilization. In A and B, error bars represent SEM between replicates, with $n = 3$. All data are representative of at least two independent experiments. P-values were calculated using Student's *t* test.

membrane microclusters that traffic centripetally toward the center of the synapse between the lymphocyte and the antigen-presenting cell (Harwood and Batista, 2010; Yokosuka and Saito, 2010). Given the similarities between NK cells and other lymphocytes, it is likely that activating NK receptors also form signaling microclusters, which would presumably need to be neutralized by inhibitory receptors to block activating responses.

In vivo, NK cells must eliminate rare target cells that are surrounded by healthy tissue expressing high levels of class I MHC. In this context, it would presumably be important to restrict the scope of inhibitory signals to avoid blocking activating responses against bona fide targets. In vitro experiments have shown that NK cells can form cytolytic synapses at one cell–cell interface while receiving inhibitory stimulation from other sites (Eriksson et al., 1999; Vyas et al., 2001), suggesting that they can indeed limit the extent of inhibitory signals. Furthermore, inhibitory killer Ig receptors (KIRs) have been observed to cluster and undergo tyrosine phosphorylation exclusively at interfaces containing their cognate MHC ligands (Davis et al., 1999; Faure et al., 2003; Vyas et al., 2004; Treanor et al., 2006). How signals emanating from these receptors are also spatially constrained, however, is not known. Also unclear is how long NK cells remain sensitive to inhibitory stimulation from before they become committed to a killing response. Precise quantification of this window of responsiveness, if it exists, would provide insight into the mechanisms that govern the integration of activating and inhibitory signals.

The analysis of signal integration in NK cells has been complicated by the speed and breadth of inhibitory responses, which make it difficult to observe interactions between activating and inhibitory pathways. To circumvent this problem, we developed a photochemical approach that enabled us to stimulate inhibitory signaling after the onset of activating signals in high-resolution imaging experiments. We prepared a semisynthetic peptide–MHC complex that is nonstimulatory to the inhibitory NK receptor KIR2DL2 until it is irradiated with UV light. Photostimulation of KIR2DL2-expressing NK cells on surfaces containing this reagent triggered the formation of inhibitory receptor microclusters and suppressed the formation of new activating receptor microclusters. This was followed by rapid reorganization of the actin cytoskeleton and retraction of the cells from the stimulatory surface. These results establish a cell biological basis for ITIM receptor signaling and provide insight into the mechanisms of signal integration in NK cells.

Results

KIR2DL2 signaling blocks the initiation of activating responses

KIR2DL2 recognizes a subset of human class I MHC molecules, including human leukocyte antigen (HLA)-Cw1, -Cw3, -Cw7, and -Cw8, and transduces inhibitory signals via two cytoplasmic ITIMs (Lanier, 2005). To analyze the effects of KIR2DL2 signaling on NK cell activation, we stably transduced the receptor into the human NK cell line NKL, which does not express any endogenous inhibitory KIR proteins (Robertson et al., 1996). To stimulate KIR2DL2 signaling, we used a mutant form of HLA-Cw3 that binds to KIR2DL2 but does not bind to ILT2, another inhibitory receptor for MHC that is expressed by NKL cells (Fig. 1 A). This HLA-Cw3 mutant, which

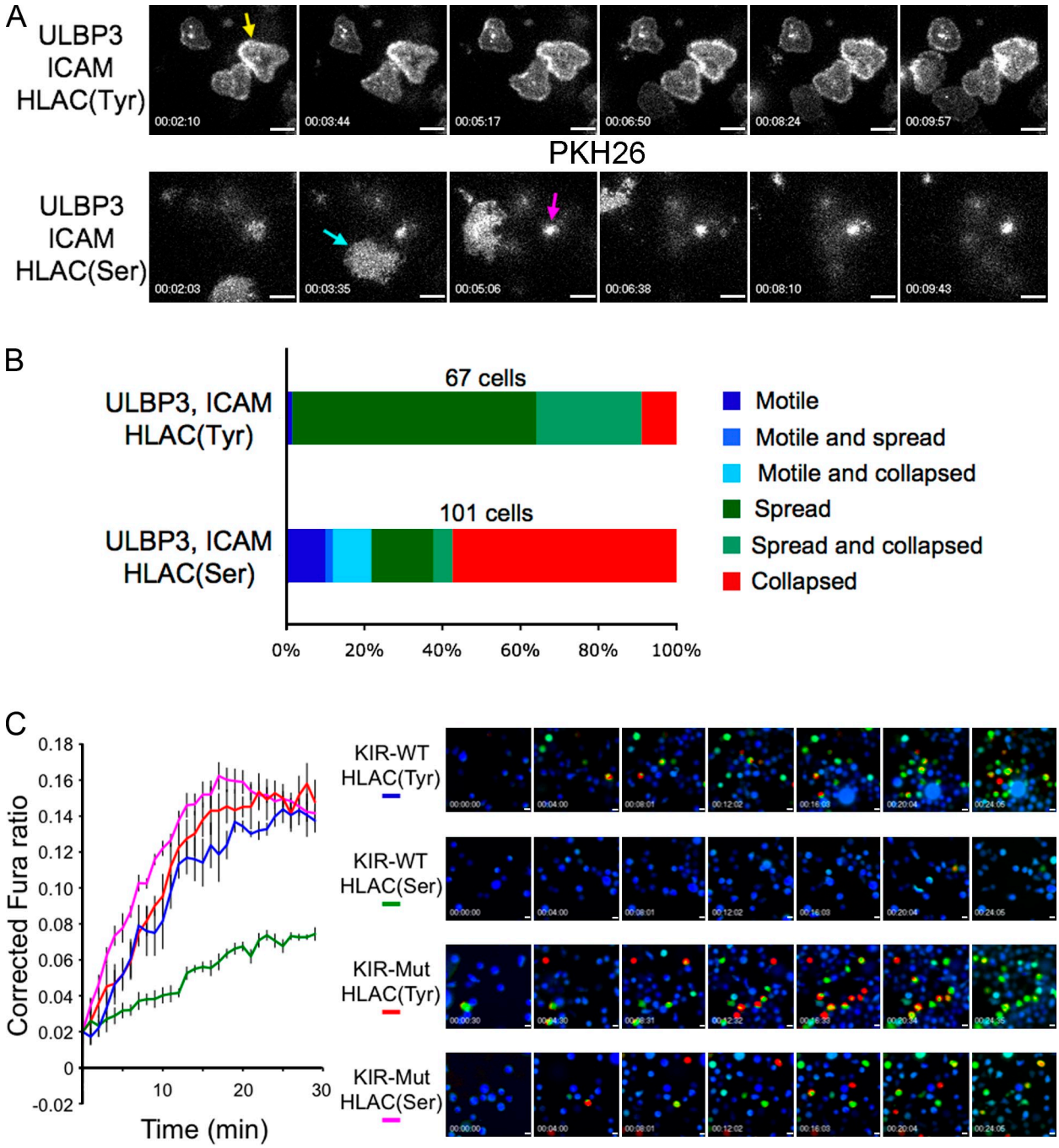

Figure 2. **KIR2DL2 signaling inhibits cell spreading and the initiation of Ca^{2+} flux.** (A and B) NKL cells expressing KIR2DL2 were stained with PKH26 and imaged using TIRF microscopy on lipid bilayers containing the indicated proteins. (A) Representative time-lapse montages (~90-s intervals) under both activating (top) and inhibitory (bottom) conditions. (B) Bar graph representing the distribution of cell behavior on surfaces containing the indicated ligands. Only cells visible in the imaging field for ≥5 min were analyzed. Cells were described as spread if they formed a stationary footprint at least 10 µm in diameter (yellow arrow in A), collapsed if they engaged in minimal dynamic interactions with the membrane (magenta arrow in A), or motile if they exhibited directional migration (cyan arrow in A). Occasionally, cells would display two phenotypes during the imaging period. (C) NKL cells expressing KIR2DL2 (KIR-WT) or KIR2DL2(mut) (KIR-Mut) were loaded with Fura-2AM and imaged on lipid bilayers containing ULBP3, ICAM, and the indicated HLA-Cw3 proteins. (right) Representative time-lapse montages (4-min intervals) showing a pseudocolored Fura-2AM ratio (warmer colors indicate higher intracellular Ca^{2+} concentrations). (left) Background-corrected mean Fura-2AM ratios for all imaging fields are plotted versus time for each condition. Error bars show SEM. All data are representative of at least two independent experiments. Bars, 10 µm.

will be called HLA-Cw3 hereafter, was purified and complexed with a nonamer peptide derived from importin-α (GAVDPLLAL). Previous experiments had demonstrated that the side chain in the p8 position of this peptide must be small (either Ala or Ser) to accommodate KIR2DL2 binding (Boyington et al., 2000). Hence, we also prepared HLA-Cw3 containing importin-α peptides with Ser or Tyr in the p8 position.

To evaluate the potency of these HLA-Cw3 reagents, we determined whether they could inhibit responses triggered by the activating receptor NKG2D. Although previous studies had

indicated that NKG2D signaling alone was insufficient to trigger NK cell activation (Bryceson et al., 2006, 2009), we found that the responsiveness of NKL cells to NKG2D was enhanced in the presence of interleukin-2 (IL-2). Under these conditions, incubation of NKL cells expressing KIR2DL2 in plastic wells coated with an antibody against NKG2D (α-NK) induced both degranulation and the secretion of IFN-γ (Fig. 1, B and C). Co-immobilization of HLA-Cw3(Ala) or HLA-Cw3(Ser) in the stimulatory wells inhibited these responses (Fig. 1, B and C). HLA-Cw3(Tyr) had no effect, confirming that a small residue in the p8 position is necessary for KIR2DL2 stimulation. NKL cells expressing a mutant of KIR2DL2 in which the crucial Tyr residues of both cytoplasmic ITIMs were replaced with Phe (called KIR2DL2(mut) hereafter) were markedly less sensitive to HLA-Cw3 (Fig. 1 D), indicating that the disruption of activating responses required ITIM signaling from KIR2DL2.

To examine the cell biological basis for this inhibition, we stained KIR2DL2-expressing NKL cells with the vital membrane dye PKH26 and imaged them using total internal reflection fluorescence (TIRF) microscopy as they interacted with supported lipid bilayers containing activating and inhibitory ligands. Consistent with previous work (Culley et al., 2009; Liu et al., 2009), NKL cells formed stable, synapselike contacts on bilayers containing ULBP3 (an NKG2D ligand), the intercellular adhesion molecule (ICAM), and the nonfunctional HLA-Cw3(Tyr) (Fig. 2, A and B; and Video 1). Substitution of HLA-Cw3(Tyr) with the functional HLA-Cw3(Ser) dramatically altered this spreading behavior; most cells did not spread at all, instead forming small, dynamic contacts (Fig. 2, A and B; and Video 2). A subset of cells exhibited a highly mobile crawling phenotype (Fig. 2 A, cyan arrow), which was consistent with the notion that inhibitory receptors block the ability of activating signals to arrest cell motility (Culley et al., 2009).

Activating bilayers also induced robust Ca^{2+} flux in KIR2DL2-expressing NKL cells. This response was blocked in the presence of HLA-Cw3(Ser) (Fig. 2 C). NKL cells expressing KIR2DL2(mut) were insensitive to HLA-Cw3(Ser), indicating that inhibition required KIR2DL2 signaling (Fig. 2 C). Collectively, these data showed that KIR2DL2-mediated inhibition of cytokine secretion and degranulation was associated with a block in the initiation of cell spreading and Ca^{2+} flux.

A photocaged ligand for KIR2DL2

The lack of observable activating responses in the presence of inhibitory ligands (Figs. 1 and 2) complicated our attempts to analyze the cellular mechanisms of inhibitory signaling. To circumvent this issue, we developed a photochemical approach that allowed us to stimulate KIR2DL2 after activating signals had begun.

As stated in the previous section, the side chain in the p8 position of the importin-α peptide must be small to allow KIR2DL2 binding to HLA-Cw3 (Boyington et al., 2000). Accordingly, we synthesized a derivative of the peptide containing a photocaged Ser residue (Veldhuyzen et al., 2003) in the p8 position (Figs. 3 A and S1), reasoning that the presence of a bulky caging group would sterically block KIR2DL2 binding to HLA-Cw3 and that UV irradiation would relieve this blockade. Indeed, HLA-Cw3 containing the photocaged peptide

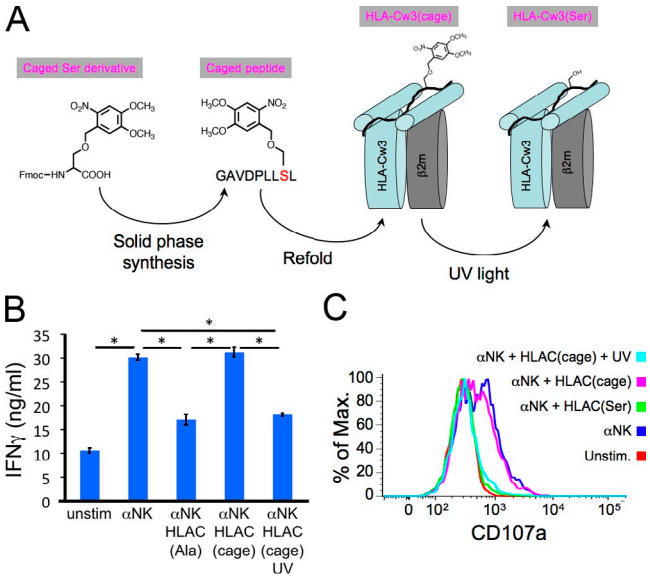

Figure 3. **Preparation of photocaged HLA-Cw3.** (A) Photocaged Ser was synthesized and incorporated into the importin-α peptide, which was then refolded with purified HLA-Cw3 and β2m. UV irradiation of HLA-Cw3(cage) yields stimulatory HLA-Cw3(Ser). (B and C) IFN-γ secretion (B) and degranulation (C) of KIR2DL2-expressing NKL cells stimulated on plastic surfaces coated with the indicated activating and inhibitory molecules. HLA-Cw3(cage) was either UV irradiated or left untreated before immobilization on the stimulatory surfaces. Asterisks in B denote $P < 0.001$ (Student's *t* test). Unstim, unstimulated. Error bars show SEM between replicates, with $n = 3$. Data are representative of at least three independent experiments.

(HLA-Cw3(cage)) had little to no effect on IFN-γ secretion and degranulation induced by activating ligands (Fig. 3, B and C). However, substantial inhibition was observed if the peptide–MHC was exposed to UV light before NK cell stimulation (Fig. 3, B and C), indicating that HLA-Cw3(cage) is a photoinducible ligand for KIR2DL2.

KIR2DL2 photostimulation induces receptor microcluster formation and cellular retraction

Having validated that HLA-Cw3(cage) could induce UV-dependent inhibitory signaling, we used this reagent in imaging experiments to stimulate KIR2DL2 during ongoing activating responses (Fig. S2 A). NKL cells expressing GFP-labeled KIR2DL2 were imaged by TIRF microscopy on bilayers containing ULBP3, ICAM, and HLA-Cw3(cage). These bilayers induced symmetric cell spreading characteristic of activation, reflecting the fact that HLA-Cw3(cage) does not inhibit activating responses before UV exposure (Fig. 4 A and Video 3). Subsequent UV irradiation of the surface induced the rapid (<3 s) formation of KIR2DL2 microclusters, particularly in an annular zone at the periphery of the contact (Figs. 4, A and B; and S2 B; and Video 3). This was followed, in most experiments, by the retraction of the cell from the bilayer. Retraction occurred primarily in the peripheral region enriched in KIR2DL2 microclusters, and the process tended to eliminate these clusters. In most experiments, we observed low levels of UV-independent KIR2DL2 clustering on membranes containing HLA-Cw3(cage) (Fig. 4 A), which was most likely a result of background levels

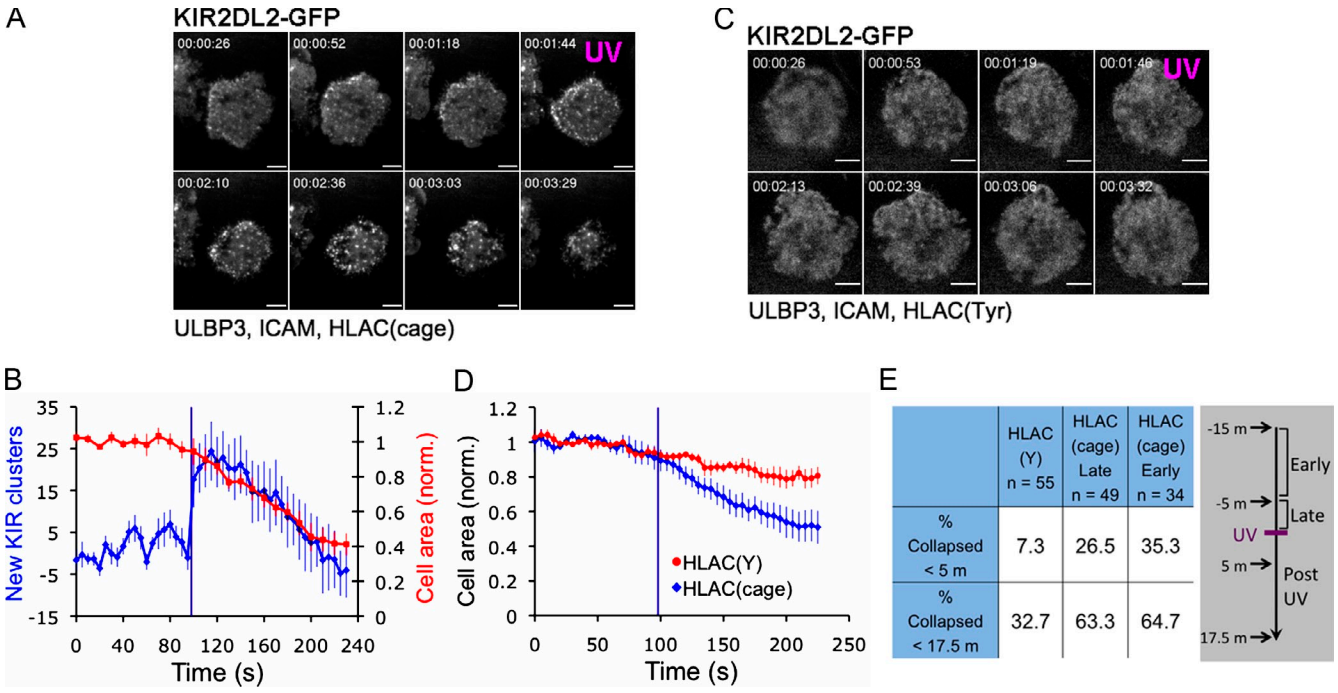

Figure 4. **Photostimulation of KIR2DL2 induces receptor microclusters and cellular retraction.** (A–D) NKL cells expressing KIR2DL2-GFP were imaged using TIRF microscopy and UV irradiated on bilayers containing ULBP3, ICAM, and either HLA-Cw3(Tyr) or HLA-Cw3(cage). (A and C) Representative time-lapse montages (~25-s intervals) showing NKL cells responding to photostimulation on surfaces containing the indicated proteins. UV irradiation is denoted in magenta. (B) Graph showing the change in KIR2DL2 microclusters and cell contact area after photostimulation on bilayers containing HLA-Cw3(cage). Data were derived from seven cells. (D) Graph showing mean cell contact area before and after photostimulation on bilayers containing the indicated HLA-Cw3 proteins. Each curve was derived from at least nine cells. (E) PKH26-stained NKL cells expressing KIR2DL2 were imaged on bilayers containing ULBP3, ICAM, and the indicated HLA-Cw3 proteins for up to 15 min before UV irradiation. Cells on the HLA-Cw3(cage) bilayer were grouped based on when they formed stable contacts with the bilayer (early, first 5 min; late, between 5 and 15 min) and how quickly they collapsed after UV (within 5 or 17.5 min). A timeline for the experiment is shown on the right in a gray box. Cells were defined as collapsed once their footprint on the bilayer shrank to <50% of its value before UV irradiation. Error bars represent SEM. Purple lines in graphs denote UV irradiation. All data are representative of at least two independent experiments. norm., normalized. Bars, 5 µm.

of decaging that were insufficient to promote retraction. Importantly, photostimulation on bilayers containing HLA-Cw3(Tyr) instead of HLA-Cw3(cage) induced neither KIR2DL2 clustering nor cellular retraction, indicating that both responses required HLA-Cw3(cage) (Fig. 4, C and D).

To better characterize the speed and prevalence of retraction after KIR2DL2 stimulation, we performed lower resolution TIRF experiments in which multiple cells were imaged simultaneously. PKH26-labeled NKL cells expressing KIR2DL2 were allowed to spread on bilayers containing ULBP3, ICAM, and either HLA-Cw3(Tyr) or HLA-Cw3(cage) for a defined period of time and then UV irradiated as a group. KIR2DL2-mediated retraction tended to be quite rapid. Of the cells that collapsed in response to photostimulation (~65% of total cells), close to half did so within 5 min of UV exposure (Fig. 4 E). We also asked how the duration of activating signals before photostimulation affected subsequent retraction responses to investigate whether there was a finite period of sensitivity to inhibitory signals. Our data, which included cells that landed up to 15 min before UV irradiation, revealed no evidence for a loss in responsiveness over time (Fig. 4 E). Hence, NK cells retract within minutes of KIR2DL2 stimulation, and they remain sensitive to inhibitory signals at least 15 min after initial activation.

Photostimulation experiments were also performed using cultured primary human NK cells expressing KIR2DL3, which is closely related to KIR2DL2 and shares the same ligand specificity (Lanier, 2005). These cells spread and fluxed Ca^{2+} on bilayers containing ULBP3 and ICAM as the sole activating ligands (unpublished data), which was consistent with previous studies showing that culturing NK cells in IL-2 enhances NKG2D expression and responsiveness (Bryceson et al., 2006; Decot et al., 2010). Importantly, UV irradiation on bilayers containing HLA-Cw3(cage), but not HLA-Cw3(Tyr), induced cellular retraction (Fig. 5). These responses were qualitatively similar to those observed with NKL cells but tended to be weaker quantitatively. This could be caused by differences in the inhibitory potency of KIR2DL3 relative to KIR2DL2. It is also possible that primary NK cells express a composition of cytoplasmic signaling regulators that makes them less responsive to inhibitory stimulation than NKL cells. Nevertheless, these results indicate that the retraction response to inhibitory KIR stimulation is not unique to the NKL cell line.

ITIM signaling is required for retraction but not microcluster formation

To determine whether KIR2DL2 microcluster formation and cellular retraction required KIR2DL2 signaling, we photostimulated NKL cells expressing KIR2DL2(mut)-GFP. KIR2DL2(mut) formed microclusters in response to photostimulation that were enriched in the periphery of the contact, similar to wild-type

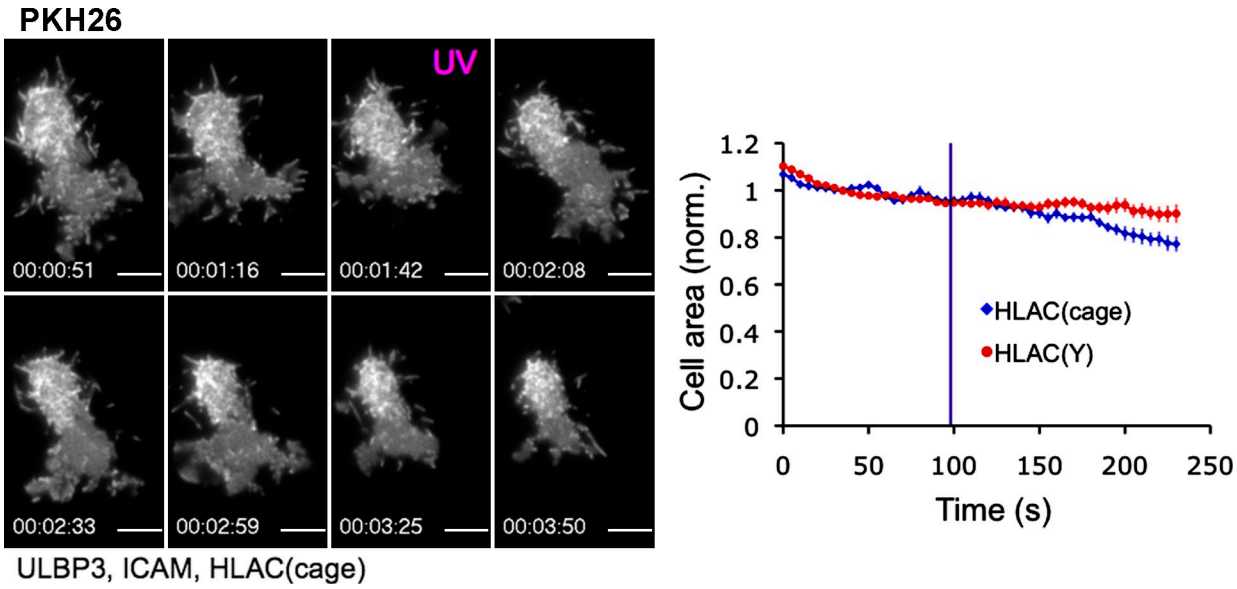

Figure 5. **Photostimulation of KIR2DL3 triggers retraction in primary human NK cells.** KIR2DL3$^+$ NK cells were stained with PKH26 and photostimulated on bilayers containing ULBP3, ICAM, and either HLA-Cw3(cage) or HLA-Cw3(Tyr). (left) A time-lapse montage (~25-s intervals) showing a representative photostimulation experiment on a bilayer containing HLA-Cw3(cage). UV irradiation is indicated in magenta. (right) A graph showing the mean cell contact area before and after photostimulation on bilayers containing the indicated HLA-Cw3 proteins. The purple line denotes UV irradiation. Each curve was derived from ≥15 cells. Error bars show SEM. Data are representative of two independent experiments. norm., normalized. Bars, 5 µm.

KIR2DL2 (Figs. 6, A and B; and S2 C; and Video 4). However, no significant retraction was observed, and peripheral microclusters tended to persist for the duration of the experiment. Hence, ITIM signaling is required for retraction but not for KIR2DL2 microcluster formation.

In NK cells, ITIM-induced dephosphorylation of activating signaling proteins is mediated by SHP-1 and SHP-2 (Burshtyn et al., 1996; Olcese et al., 1996). To assess the role of these phosphatases downstream of KIR2DL2, photostimulation experiments were performed in the presence of NSC87877, a SHP-1/2 inhibitor. NSC87877 substantially impaired retraction responses but did not affect KIR2DL2 microcluster formation (Figs. 6 C and S2 D), suggesting that recruitment and activation of SHP-1/2 is required for mediating ITIM-induced changes in synaptic structure.

The actin motor protein myosin II has been implicated in retraction responses in several systems (Small and Resch, 2005). However, KIR2DL2-induced collapse of the contact region was unaffected by the myosin inhibitor blebbistatin (Fig. S2 E), suggesting that it operates via a myosin-independent mechanism.

KIR2DL2 signaling induces remodeling of the actin cytoskeleton

The observation that KIR2DL2 photostimulation triggered retraction suggested that ITIM signaling might be altering the underlying actin cytoskeleton. Cytolytic synapse formation is accompanied by a burst of actin polymerization (Orange et al., 2003), and agents that disrupt filamentous actin block killing and other activating responses (Watzl and Long, 2003; Barber et al., 2004; Endt et al., 2007). Previous studies have demonstrated that actin accumulates in an annular zone at the periphery of the synapse (Bunnell et al., 2001; Arana et al., 2008; Culley et al., 2009), where it is thought to be important for cell spreading and target cell adhesion.

To investigate the effects of ITIM receptor signaling on actin structure, we transduced NKL cells with the Lifeact peptide (Riedl et al., 2008), which binds specifically to filamentous actin. When cells expressing KIR2DL2-GFP and Lifeact-RFP contacted bilayers containing ULBP3, ICAM, and HLA-Cw3(cage), the Lifeact-RFP probe accumulated in a ring at the periphery of the synapse, which is characteristic of an activated lymphocyte. Subsequent UV irradiation dramatically altered this configuration (Fig. 7 A and Video 5). As the contact retracted, the actin ring "filled in" so that the intensity of the Lifeact-RFP probe became uniform over the entire interface. UV-induced dissolution of the actin ring was far less frequent on bilayers containing HLA-Cw3(Tyr) instead of HLA-Cw3(cage) (Fig. 7 B). This remodeling response was also impaired by NSC87877 (Fig. 7 C). Hence, the reorganization of actin induced by KIR2DL2 requires both ITIM signaling and SHP-1/2 activity.

"Outside-in" signals from integrins play an important role in leukocyte adhesion and cell spreading by promoting the polymerization and stabilization of actin (Abram and Lowell, 2009). To determine whether integrin signaling to the cytoskeleton could counteract the effects of KIR2DL2, we performed photostimulation experiments in the presence of manganese (Mn^{2+}), a divalent cation that up-regulates integrin-mediated adhesion and enhances outside-in signaling. Indeed, UV-induced retraction was diminished by Mn^{2+} treatment (Fig. S3), suggesting that integrin and KIR2DL2 signals intersect at the level of actin. Interestingly, however, Mn^{2+} did not block the dissolution of the peripheral actin ring (Fig. 7 D). Hence, there are certain aspects of KIR2DL2-mediated actin remodeling that are not reversed by integrin signaling.

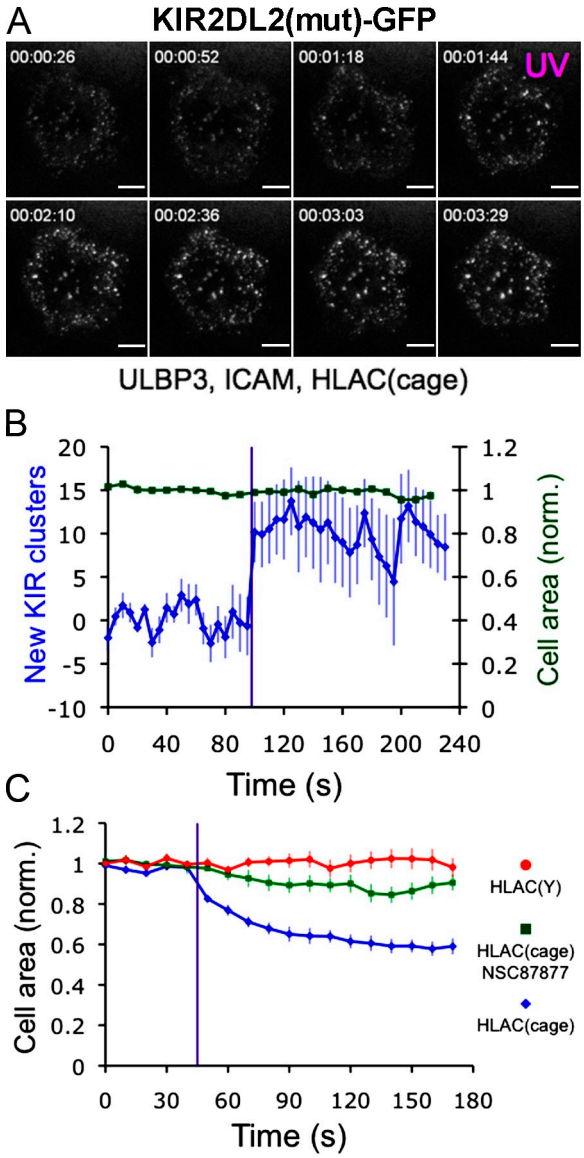

Figure 6. **ITIM signaling and SHP-1/2 activity are required for cellular retraction.** (A and B) NKL cells expressing KIR2DL2(mut)-GFP were imaged using TIRF microscopy and UV irradiated on bilayers containing ULBP3, ICAM, and HLA-Cw3(cage). (A) Time-lapse montage (~25-s intervals) showing a representative response UV irradiation, which is indicated in magenta. (B) Graph showing the cell contact area and the change in KIR2DL2 microcluster number after photostimulation. Data were derived from 12 cells. (C) NKL cells expressing wild-type KIR2DL2 were photostimulated on bilayers containing ULBP3, ICAM, and the indicated HLA-Cw3 proteins in the presence or absence of NSC87877. Mean cell contact area is graphed both before and after UV irradiation. Each curve was derived from at least seven cells. Throughout the figure, purple lines indicate UV irradiation. Error bars show SEM. All data are representative of at least two independent experiments. norm., normalized. Bars, 5 µm.

The activating receptor NKG2D forms ligand-dependent microclusters

The aforementioned imaging experiments showed that KIR2DL2 stimulation could reverse cell-spreading responses induced by the activating receptor NKG2D. To visualize NKG2D dynamics directly, we fluorescently labeled DAP10, a small signaling adaptor that constitutively associates with NKG2D (Lanier, 2005). When NKL cells expressing DAP10-GFP were added to lipid bilayers containing ULBP3 and ICAM, microclusters of DAP10 formed that could be imaged by TIRF microscopy (Fig. 8 A and Video 6). These microclusters were not observed on bilayers containing ICAM alone (Fig. S4), indicating that they required NKG2D stimulation. Microclusters adopted one of two behaviors (Fig. 8 A). One group of clusters formed in the periphery and migrated centripetally toward the center of the contact. The second group was relatively immobile and tended to be distributed closer to the central region. The mobile clusters either vanished as they approached the center or merged with other clusters and became immobile (Video 6). Interestingly, neither the immobile nor the mobile clusters fused into a single central accumulation over time. This distinguishes NKG2D-DAP10 microclusters from antigen receptor microclusters in T cells and B cells, which coalesce into a central supramolecular activation cluster as the synapse matures (Harwood and Batista, 2010; Yokosuka and Saito, 2010).

To determine which pool of DAP10 microclusters was actively engaged in signaling, we imaged DAP10-GFP–expressing NKL cells that were fixed on bilayers containing ULBP3 and ICAM and then stained with antibodies against phosphotyrosine. Although microclusters near the center of the contact tended to contain more DAP10, phosphotyrosine staining was enriched in the peripheral microclusters (Fig. 8, B–D). These results, which are similar to what has been observed for antigen receptor clusters in T cells (Campi et al., 2005; Yokosuka et al., 2005; Varma et al., 2006), suggested that signaling is mediated predominantly by peripheral clusters containing NKG2D-DAP10.

KIR2DL2 signaling inhibits the formation of activating receptor microclusters

Next, we imaged DAP10-GFP and KIR2DL2-mCherry in the same cells to assess the interplay between the two receptors. As described in previous sections, photostimulation on bilayers containing ULBP3, ICAM, and HLA-Cw3(cage) induced the rapid formation of KIR2DL2 microclusters, particularly in the periphery of the contact. This ring of KIR2DL2 showed little overlap with the relatively stable immobile pool of DAP10 clusters located in the central region (Fig. 9 A). Indeed, many of these immobile DAP10 clusters persisted for the duration of the retraction response, even as the annular zone of KIR2DL2 accumulation collapsed inward. In contrast, KIR2DL2 stimulation dramatically affected the mobile pool of DAP10 microclusters in the periphery. Although these clusters were readily apparent before photostimulation (Fig. 9 A, arrows), they tended to be absent after UV irradiation, particularly in peripheral regions rich in KIR2DL2 (Fig. 9 A, brackets). Particle tracking revealed that the formation of peripheral DAP10 clusters was strongly inhibited by UV irradiation (Fig. 9, B and C; and Video 7). Peripheral clusters were not suppressed by UV irradiation on surfaces containing HLA-Cw3(Tyr) instead of HLA-Cw3(cage) (Fig. 9, B and C), indicating that the response required KIR2DL2 stimulation. Hence, the formation of KIR2DL2 microclusters at the periphery of the synapse is associated with the suppression of new DAP10 microclusters in the same domain.

Because we had also observed that KIR2DL2 photostimulation alters actin structure (Fig. 7), we explored the possibility that

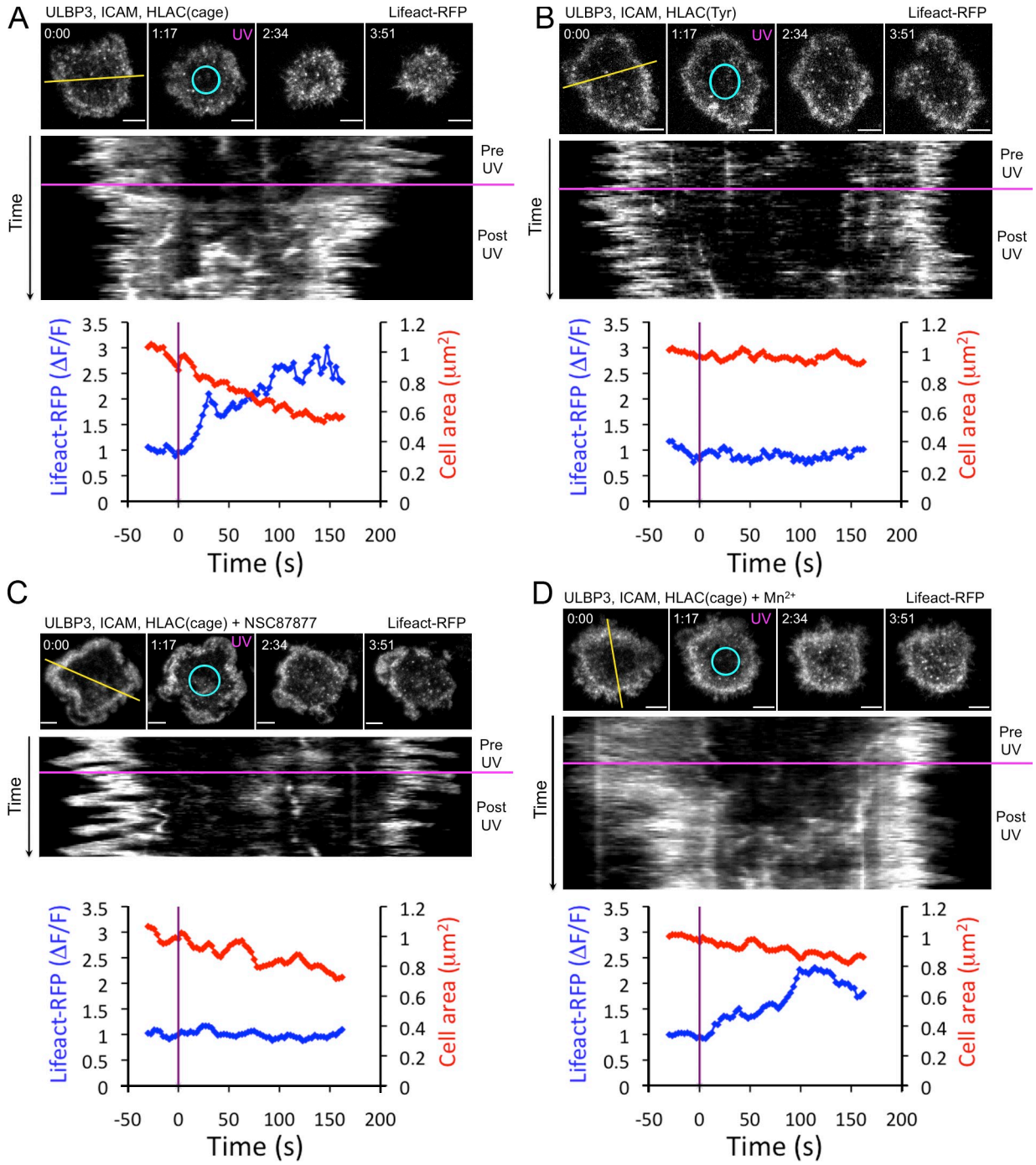

Figure 7. **KIR2DL2 photostimulation induces actin remodeling.** (A–D) NKL cells expressing KIR2DL2 and Lifeact-RFP were imaged using TIRF microscopy and UV irradiated on bilayers containing ULBP3, ICAM, and either HLA-Cw3(cage) (A, C, and D) or HLA-Cw3(Tyr) (B). Photostimulation was performed using cells left untreated (A and B) or treated with NSC87877 (C) or Mn^{2+} (D). For each panel, a time-lapse montage (~75-s intervals) is shown (top) along with an associated kymograph. UV irradiation is indicated by magenta text in the time lapse and by a magenta line in the kymograph. Kymographs were generated using the yellow line in the first image of each time lapse. Shown on the bottom in each panel, normalized mean fluorescence intensity of Lifeact-RFP in the center of the contact is graphed as a function of time together with cell area. The contact center is indicated by a cyan ellipse in each time lapse. Data are representative of at least two independent experiments. ΔF/F, normalized fluorescence intensity. Bars, 5 μm.

actin is required for DAP10 microcluster dynamics. NKL cells expressing DAP10-GFP were imaged on bilayers containing ULBP3 and ICAM both before and after the addition of the actin-depolymerizing agent latrunculin. Treatment with latrunculin abolished the formation and centripetal migration of peripheral DAP10 microclusters (Fig. 9, C and D), indicating that filamentous actin is necessary for NKG2D-DAP10 microcluster assembly and trafficking. These results are similar to what has been observed for antigen receptor microclusters in T cells (Varma et al., 2006). Collectively, our data indicated that KIR2DL2 signaling inhibits activating receptor microcluster formation, possibly by influencing the underlying actin cytoskeleton.

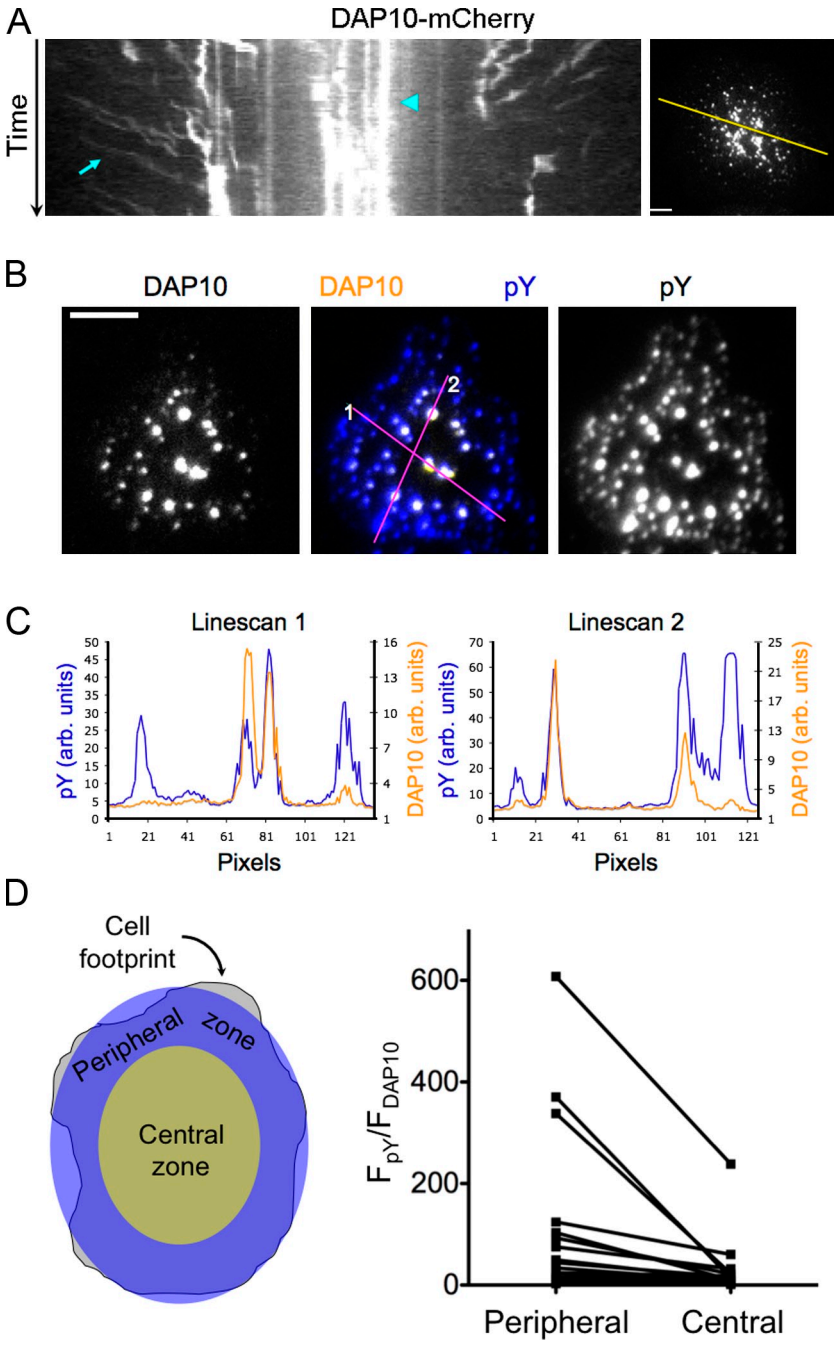

Figure 8. **NKG2D stimulation induces the formation of activating receptor microclusters.** (A) NKL cells expressing DAP10-mCherry were imaged using TIRF microscopy on bilayers containing ULBP3 and ICAM. (left) A kymograph showing centripetally mobile and stationary DAP10 clusters, indicated by the cyan arrow and arrowhead, respectively. The line used to generate the kymograph is shown on the right. (B–D) NKL cells expressing DAP10-GFP were fixed and stained with antibodies against phosphotyrosine (pY) on bilayers containing ULBP3 and ICAM. (B) Representative images showing DAP10 fluorescence (left), phosphotyrosine fluorescence (right), and the overlay (center). (C) Linescans depicting DAP10 and phosphotyrosine fluorescence (yellow and blue, respectively) in specific microclusters within the contact region. The lines used for each linescan are shown in the central image in B. (D, left) Schematic showing how images were divided into central and peripheral zones for quantification. (right) Before and after graph showing the ratio of normalized phosphotyrosine fluorescence intensity (F_{pY}) to normalized DAP10-GFP fluorescence intensity (F_{DAP10}) for peripheral and central regions. Ratios calculated from the same cell are connected by lines. All data are representative of at least two independent experiments. arb., arbitrary. Bars, 5 µm.

KIR2DL2 signaling does not block ongoing calcium responses

We also examined the ability of KIR2DL2 photostimulation to inhibit ongoing Ca^{2+} responses. NKL cells expressing KIR2DL2 displayed robust Ca^{2+} flux upon contact with bilayers containing ULBP3, ICAM, and either HLA-Cw3(Tyr) or HLA-Cw3(cage) (Fig. 10 A). Intracellular Ca^{2+} concentrations typically peaked in the first few minutes of the response before entering a phase of sustained Ca^{2+} elevation (Fig. 10 B). UV irradiation, which we delivered during the sustained phase in some cells and the early phase in others, did not significantly affect the intensity of Ca^{2+} responses on HLA-Cw3(cage) surfaces relative to HLA-Cw3(Tyr) controls (Fig. 10, A and B). Mean Ca^{2+} levels on both surfaces after UV irradiation were essentially superimposable (Fig. 10 C).

That KIR2DL2 photostimulation did not inhibit ongoing Ca^{2+} responses was surprising, given that KIR2DL2 did block the initiation of Ca^{2+} flux when triggered concurrently with activating receptors (Fig. 2 C). We sought to confirm this observation using a flow cytometry–based approach. NKL cells expressing KIR2DL2 were preincubated with biotinylated mouse antibodies against two activating receptors, NKG2D and 2B4, either in the presence or absence of an unbiotinylated mouse antibody against KIR2DL2. Streptavidin (SA) was then used to trigger activating signals and an anti–mouse secondary antibody (α-Mouse) to induce inhibition (Fig. S5). Consistent with previous

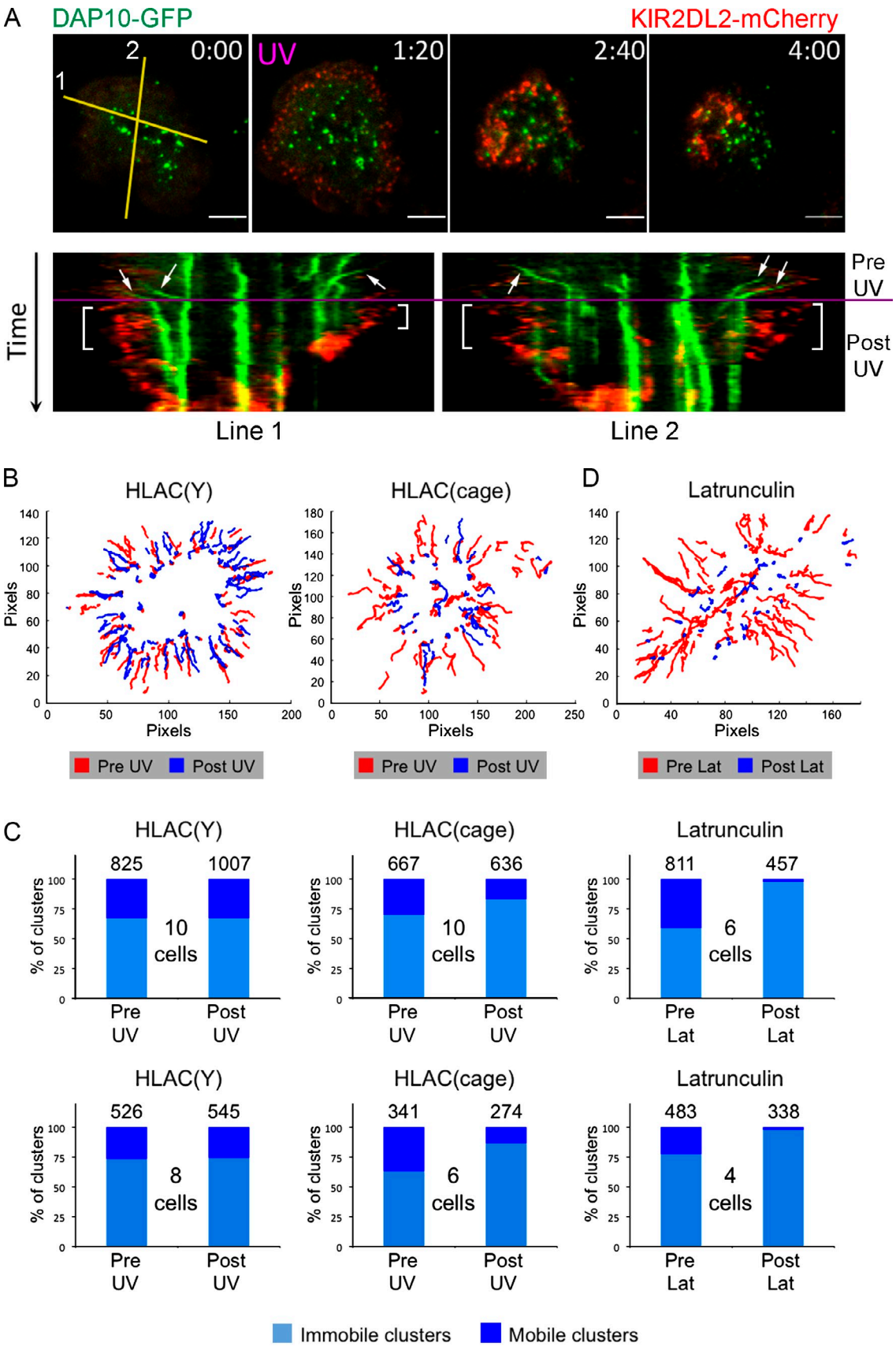

Figure 9. **KIR2DL2 photostimulation blocks the formation of activating receptor microclusters.** (A) NKL cells expressing DAP10-GFP and KIR2DL2-mCherry were imaged in TIRF mode and photostimulated on bilayers containing ULBP3, ICAM, and HLA-Cw3(cage). (top) A representative time-lapse montage (~80-s intervals), with UV irradiation indicated by magenta text. (bottom) Two single-cell kymographs showing KIR2DL2-mCherry and DAP10-GFP clusters

studies (Binstadt et al., 1996; Bléry et al., 1997; Bruhns et al., 1999; Bryceson et al., 2006), clustering of NKG2D and 2B4 with SA induced rapid Ca^{2+} flux (Fig. 10 D). This response was inhibited by simultaneous co–cross-linking of KIR2DL2, but not KIR2DL2(mut), with α-Mouse, indicating that KIR2DL2 signaling impairs the initiation of Ca^{2+} responses (Fig. 10 D, top). To test whether KIR2DL2 could inhibit ongoing Ca^{2+} responses, α-Mouse was added either 75 or 150 s after initial NKG2D and 2B4 cross-linking. Only weak inhibition was observed relative to control cells in both of these experiments (Fig. 10 D, bottom). These data confirmed that whereas KIR2DL2 can inhibit the induction of Ca^{2+} flux, it is substantially less effective at curtailing ongoing Ca^{2+} responses.

Discussion

The cell biological basis of ITIM receptor signaling in NK cells has remained largely unexplored because of difficulties in visualizing inhibitory and activating signals simultaneously. Using a photoinducible ligand for KIR2DL2, we were able to separate the stimulation of activating and inhibitory pathways in time and establish a spatial and temporal window of sufficient size to actually observe interactions between them. Our work provides insight into the mechanisms of ITIM receptor signaling and signal integration in NK cells.

Photostimulation of KIR2DL2 during ongoing activating responses is admittedly an imperfect model for the simultaneous triggering of activating and inhibitory receptors that presumably occurs in many NK cell–target cell synapses. Nevertheless, we feel that our results reflect a biologically relevant mechanism for ITIM receptor signaling for the following reasons. First, the retraction response we observe requires ITIM signaling and SHP-1/2 activity, the same molecular determinants necessary for KIR-mediated inhibition in other systems. Second, our observation that NK cells remain responsive to inhibitory stimulation well after the onset of activating signals is consistent with previous experiments showing that NK cells modify the morphology of a growing synapse upon encountering ITIM receptor ligands (Culley et al., 2009). In vivo, the ability to respond to fresh inhibitory stimulation in this manner is likely important for keeping growing cytolytic synapses with bona fide targets from spilling over onto adjacent bystander cells.

Pioneering imaging studies in T cells have indicated that activating signals are initiated by antigen receptor microclusters at the periphery of the synapse and that, in most cases, signaling is down-regulated as these clusters approach the center (Campi et al., 2005; Mossman et al., 2005; Yokosuka et al., 2005; Varma et al., 2006). Thus, sustained signaling is dependent on the continuous formation of new peripheral microclusters. Using DAP10 as a probe, we observed that the NKG2D receptor complex forms two kinds of clusters, a mobile variety that is generated in the periphery and migrates centripetally and an immobile variety that accumulates closer to the center. Interestingly, NKG2D-DAP10 does not coalesce into a central supramolecular activation cluster over time, possibly because NKG2D signaling is mediated by Tyr-Ile-Met-Asn motifs in DAP10 rather than the immunotyrosine-based activation motifs contained in antigen receptors. Nevertheless, peripheral DAP10 microclusters contain higher levels of phosphotyrosine, suggesting that they mediate most of the NKG2D-dependent signaling. Strikingly, it is in this peripheral zone that we observed UV-induced accumulation of KIR2DL2 microclusters, suppression of DAP10 microclusters, and actin remodeling.

It is well established that filamentous actin at the synapse is required for receptor-proximal activating signals in NK cells (Orange et al., 2003; Watzl and Long, 2003; Barber et al., 2004; Endt et al., 2007). Consistent with these studies, we observed that disrupting synaptic actin with latrunculin blocked DAP10 microcluster formation and movement. Interestingly, when cells were subjected to KIR2DL2 photostimulation, suppression of activating microclusters occurred within seconds, before the dissolution of the peripheral actin ring, indicating that cytoskeletal retraction per se is not responsible for microcluster suppression. It is possible, however, that the dramatic actin reorganization induced by KIR2DL2 signaling is preceded by a period of actin destabilization that is more difficult to detect and that this initial actin destabilization is sufficient to suppress activating microclusters.

The pathway linking inhibitory receptors to actin remodeling remains unclear but is likely to involve Vav-1, a guanine nucleotide exchange factor that is phosphorylated and activated during synapse formation (Bustelo, 2000; Riteau et al., 2003). Vav-1 stimulates the Rho family GTPase Rac1, which is thought to promote cytolytic function and target cell adhesion by triggering actin polymerization and the up-regulation of integrins (Billadeau et al., 1998; Galandrini et al., 1999; Riteau et al., 2003; Nolz et al., 2008). It is known that SHP-1 directly dephosphorylates Vav-1 downstream of ITIM receptors (Stebbins et al., 2003), which could conceivably lead to the actin remodeling we have observed.

Integrins play a critical role in NK cell function by promoting synapse formation and the polarization of cytolytic granules (Barber et al., 2004; Bryceson et al., 2005). Our observations that KIR2DL2 signaling induced retraction and that

both before and after UV irradiation, which is indicated by the magenta line. Mobile clusters of DAP10 are denoted by arrows. Brackets indicate areas of the kymographs showing peripheral regions rich in KIR2DL2 microclusters but devoid of mobile DAP10 microclusters. Lines used for kymographs are shown in the first image of the time lapse. (B and D) Tracks of DAP10 microclusters in representative single cells. (B) Cells were imaged and UV irradiated on bilayers containing ULBP3, ICAM, and either HLA-Cw3(Tyr) (left) or HLA-Cw3(cage) (right). Paths traveled before UV irradiation are shown in red, and paths after UV irradiation are shown in blue. (D) Cells were treated with latrunculin (Lat) on bilayers containing ULBP3 and ICAM. Paths traveled before latrunculin addition are shown in red, and paths after latrunculin addition are shown in blue. (C) Bar graphs showing the relative amounts of mobile versus immobile DAP10 microclusters. (left and center) Cells were photostimulated on bilayers containing either HLA-Cw3(Tyr) (left) or HLA-Cw3(cage) (center). (right) Cells were treated with latrunculin on bilayers containing ULBP3 and ICAM. The total number of analyzed microclusters is indicated above each bar, and the number of analyzed cells for each experiment is shown between bars. The mean starting ratio of mobile to immobile microclusters differed from experiment to experiment. Hence, two independent experiments, each derived from cells imaged the same day, are shown for each condition. Bars, 5 µm.

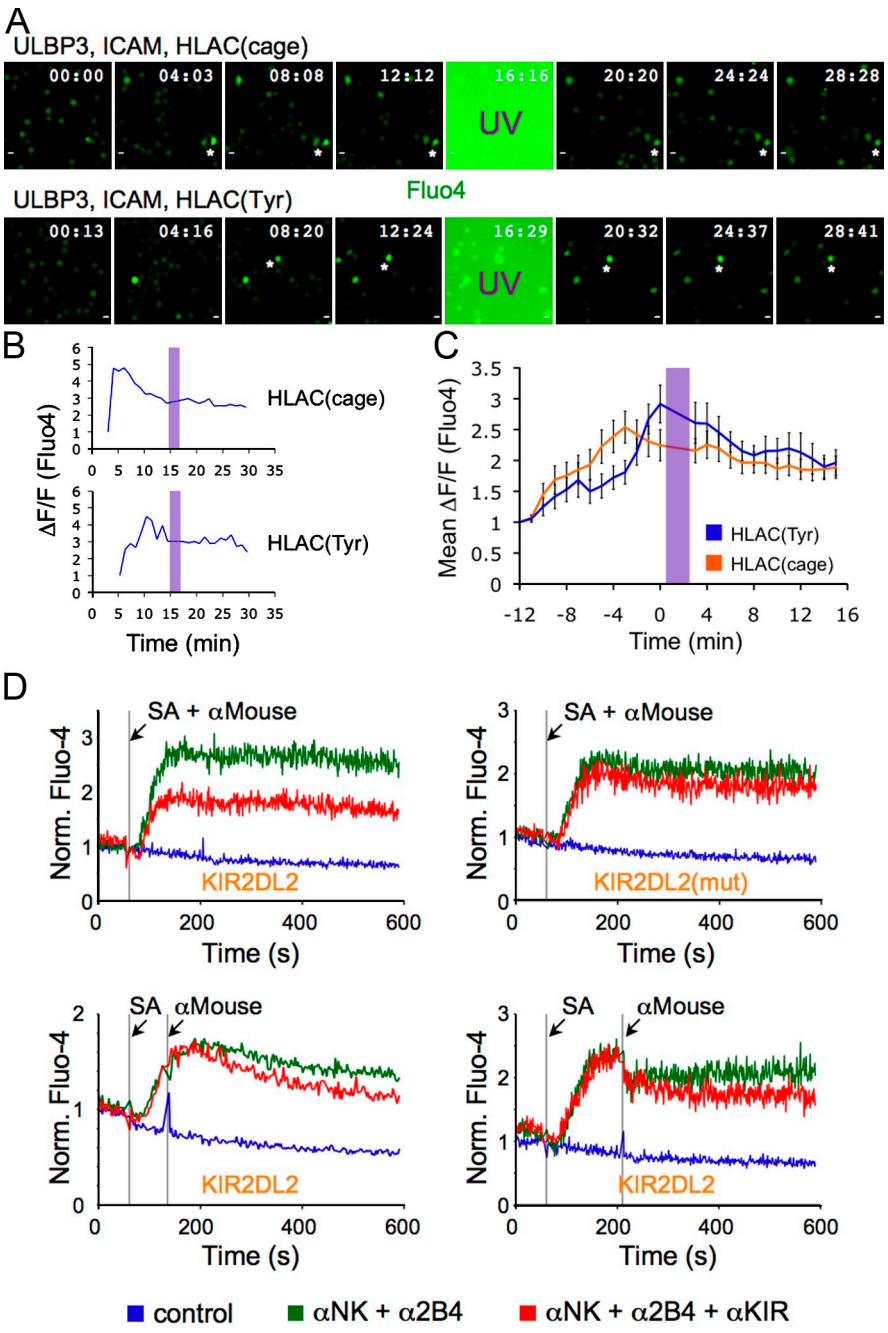

Figure 10. **Photostimulation of KIR2DL2 does not block ongoing Ca^{2+} responses.** Fluo-4AM–loaded NKL cells expressing KIR2DL2 were imaged and UV irradiated on bilayers containing the indicated proteins. (A) Time-lapse montages (~4-min intervals) showing Fluo-4AM responses before and after UV irradiation. Fluo-4AM fluorescence is proportional to intracellular Ca^{2+} concentration. (B) Ca^{2+} responses of two individual cells, which are indicated by asterisks in A. (C) Mean calcium responses for the entire population of cells. Each curve was derived from ≥30 cells. Error bars show SEM. In B and C, shaded purple bars denote UV irradiation. (D) Antibody cross-linking of KIR2DL2 does not inhibit ongoing Ca^{2+} responses. Fluo-4AM–loaded NKL cells expressing either wild-type KIR2DL2 or KIR2DL2(mut) were incubated with the indicated antibodies and subjected to flow cytometry. (top) SA (to cross-link α-NK and α-2B4) and α-Mouse (to cross-link α-KIR with α-NK and α-2B4) were added simultaneously as indicated. (bottom) α-Mouse was added after SA as indicated. All data are representative of at least two independent experiments. Norm., normalized. Bars, 10 µm.

Mn^{2+} blocked this response are consistent with previous work suggesting a direct link between ITIM-dependent signaling and the regulation of integrins (Burshtyn et al., 2000; Bryceson et al., 2009). The formation and maintenance of integrin-mediated cell–cell contacts require Vav and the Rho family GTPases, and also depend on a strong physical linkage between ligand-bound integrins and the underlying actin cytoskeleton (Swat and Fujikawa, 2005; Abram and Lowell, 2009). KIR2DL2-induced actin remodeling would presumably weaken this adhesive network either by breaking contacts between integrins and the cytoskeleton or by somehow inducing affinity down-regulation of integrins. That Mn^{2+} treatment preserves the contact area in photostimulation experiments is consistent with the notion that outside-in signaling is affected by ITIM receptors, as previously suggested (Barber et al., 2004). This result also implies that there is at least some down-regulation of integrin affinity taking place in response to ITIM signaling. That Mn^{2+} does not block the dissolution of the actin ring, however, indicates that outside-in signaling alone is insufficient to counteract the effects of KIR2DL2.

Actin remodeling and concomitant retraction are well suited as mechanisms for NK cell inhibition for two reasons. First, by targeting the integrity of the synapse, which is required by most, if not all, activating receptors, actin remodeling provides an elegant way to block effector responses that is independent of the specific activating pathways involved. Second, because retraction breaks cell–cell contact and hence the receptor–ligand interactions that drive the response, it is self-limiting

and more easily constrained in space and time. This would presumably facilitate efficient scanning of potential target cells in vivo. In this context, retraction from inhibitory cells would not only prevent inappropriate killing responses but also play an important role in directing those responses to the correct targets.

Using photostimulation as well as antibody-mediated receptor cross-linking, we found that KIR2DL2 only weakly inhibits ongoing Ca^{2+} responses despite the fact that it blocks the initiation of Ca^{2+} flux when triggered concurrently with activating receptors. This result is intriguing, particularly because KIR2DL2-induced retraction was not diminished, in our hands, by prolonged exposure to activating signals. Collectively, our data suggest that strong adhesion to the target cell is required for the initiation, but not the maintenance, of Ca^{2+} signals. Precisely why KIR2DL2 stimulation does not block ongoing Ca^{2+} responses is unclear. It is possible that ITIM receptor signaling disrupts early events, such as the activation of phospholipase C, that are required for the initiation of Ca^{2+} flux but has less of an effect on store-operated calcium channels or other downstream components that have been implicated in the sustained phase of the response (Lewis, 2001). Further studies will be required to explore this issue. From a functional perspective, however, limiting the scope of KIR2DL2 action could facilitate target cell killing in vivo. Elevated cytoplasmic Ca^{2+} is required for the secretion of lytic granules (Ostergaard et al., 1987; Takayama and Sitkovsky, 1987; Esser et al., 1998). The insensitivity of ongoing Ca^{2+} responses to ITIM receptor signals would presumably allow NK cells to mount a cytolytic response at one cell–cell interface while receiving inhibitory signals at a distal contact site. This model is consistent not only with our data but also with recent experiments indicating that ITIM receptors are more effective at blocking lytic granule polarization toward the synapse than at disrupting degranulation (Das and Long, 2010).

The extent to which the cellular consequences of KIR2DL2 signaling will apply to related signaling pathways in other cell types remains to be seen. It is worth noting, however, that the effectors of phosphorylated ITIMs, SHP-1 and particularly SHP-2, are broadly expressed, as is the tyrosine kinase Ableson, which is also required for inhibitory KIR function in NK cells (Peterson and Long, 2008). Conceptually, localized retraction is an elegant mechanism for the inhibition of signals delivered by membrane-bound ligands, and it is conceivable that this mechanism would be useful in processes such as cell migration and neuronal path finding. In that regard, it is intriguing that the ITIM receptor PirB was recently shown to promote axonal collapse in sensory neurons (Atwal et al., 2008). Future mechanistic studies will be required to determine whether or not cursory similarities like these reflect a shared mechanism for the inhibitory regulation of cell–cell interactions.

Materials and methods

Peptides

9-fluorenylmethoxycarbonyl (Fmoc)–protected dimethoxy-nitrobenzyl (DMNB) Ser was synthesized essentially as previously described (Veldhuyzen et al., 2003). In brief, Fmoc-Ser allyl ester was reacted with 4,5-dimethoxy-2-nitrobenzyl trichloroacetimidate using catalytic triflic acid under anhydrous conditions to generate the DMNB-protected Ser derivative. After allyl deprotection with palladium and purification by silica gel chromatography, the Fmoc-Ser(DMNB)-OH was further purified over a cartridge (Sep-Pak C18; Waters) using a reversed-phase solvent system: 0.1% aqueous trifluoroacetic acid (solvent A) versus 90% acetonitrile plus 0.1% trifluoroacetic acid (solvent B). Purified Fmoc-Ser(DMNB)-OH was validated by electrospray mass spectrometry and nuclear magnetic resonance, and it was then incorporated into a modified importin-α peptide at the p8 position by solid-phase peptide synthesis. After trifluoroacetic acid–mediated cleavage from the resin, the caged peptide was purified by reversed-phase HPLC using a C18 column in the absence of UV detection. Other peptides were synthesized by Fmoc chemistry either by our laboratory or by the Microchemistry and Proteomics Core Facility at the Memorial Sloan-Kettering Cancer Center. To assess UV decaging, the caged importin-α peptide was irradiated for 20 min with a 365-nm light using a handheld UV lamp (UVGL-25; Thermo Fisher Scientific). The irradiated peptide was then compared with the unirradiated peptide as well as the importin-α peptide with Ser in the p8 position by analytical reversed-phase HPLC (Fig. S1).

Proteins

HLA-Cw3, β2m, and ULBP3 were isolated from inclusion bodies under denaturing conditions. HLA-Cw3 was refolded together with β2m and importin-α peptide by rapid dilution into buffer containing 100-mM Tris, pH 8.0, 400-mM arginine, 5-mM reduced glutathione, 0.5-mM oxidized glutathione, and protease inhibitors. ULBP3 was refolded by rapid dilution into buffer containing 100-mM Tris, pH 8.0, 500-mM arginine, 5-mM reduced glutathione, 2.5-mM oxidized glutathione, and protease inhibitors. After refolding, HLA-Cw3 and ULBP3 were biotinylated using the BirA enzyme and purified by size exclusion chromatography. The extracellular domain of ICAM fused to a C-terminal histidine tag and a BirA recognition sequence was expressed in SF9 cells by baculoviral transduction and purified by Ni^{2+} affinity and anion-exchange chromatography followed by BirA-mediated biotinylation and size exclusion chromatography. In general, purified proteins were stored at −20°C in the presence of 50% glycerol. It was found, however, that prolonged storage of HLA-Cw3(cage) under these conditions increased its inhibitory activity in the absence of UV light, presumably the result of slow cleavage of the DMNB group. Hence, subsequent preparations were snap frozen in liquid nitrogen and stored at −80°C.

DNA constructs

cDNAs encoding full-length KIR2DL2 (gift from L. Lanier, University of California, San Francisco, San Francisco, CA) and DAP10 were subcloned into an murine stem cell virus (MSCV) retroviral plasmid (Quann et al., 2009) upstream of either GFP, mCherry, or a Myc epitope tag. The presence of these tags on the C termini of either KIR2DL2 or DAP10 did not affect their inhibitory or activating functions, respectively. Lifeact fused to RFP (gift from R. Wedlich-Soldner, International Max Planck Research School for Molecular and Cellular Life Sciences, Munich, Germany) was subcloned as a single fragment into pMSCV. HLA-Cw3 (gift from P. Parham, Stanford University, Stanford, CA) and ULBP3, both containing C-terminal BirA recognition sequences, were expressed in *Escherichia coli* using pET28 and pET30 expression plasmids, respectively. Mutagenesis of the ITIM Tyr residues of KIR2DL2 and the ILT2 binding site of HLA-Cw3 was performed by PCR using the Quikchange protocol (Agilent Technologies). The ILT2 binding site mutation replaces amino acid residues ^{194}VSDHE^{198} of wild-type HLA-Cw3 with ^{194}RSPGF^{198}. The baculoviral expression construct for ICAM containing a C-terminal BirA recognition sequence has been previously described (Lillemeier et al., 2010), as has the human β2m expression vector (Garboczi et al., 1992).

Cell lines and retroviral transduction

NKL cells were maintained in complete RPMI 1640 (RPMI 1640 with 10% FCS) supplemented with 200 IU/ml IL-2. Retrovirus was generated using amphotropic Phoenix cells, which were grown in DME containing 10% FCS. Phoenix cells were transfected with MSCV vectors and supplementary plasmids encoding retroviral *gag* and *pol* using either calcium phosphate or transfection reagent (FuGENE; Roche). Viral supernatants were collected after 48 h at 37°C and concentrated using centrifugal filter devices (Amicon Ultra; Millipore) with a 10^5-kD molecular mass cutoff. The virus was then mixed with 10^6 NKL cells in 2 ml complete RPMI 1640 and centrifuged at 1,400 *g* for 2 h in the presence of 8 µg/ml polybrene at 30°C. After 48 h, transduction efficiency was assessed by flow cytometry (LSR II; BD) using either the transduced fluorescent protein label or an antibody against KIR2DL2/3 (clone DX27; BD) for detection. NKL cells expressing the transduced protein (typically representing 2–10% of the total population) were isolated by FACS 1–2 wk after transduction and maintained as stable cell lines.

Primary human NK cells were isolated from peripheral blood from a healthy donor by negative selection (Miltenyi Biotec). NK cells were resuspended in stem cell growth media (CellGro; CellGenix) supplemented with 10% human serum and 200 IU/ml IL-2, and they were split periodically to maintain a density of 10^6 cells/ml. After ≥8 d at culture, KIR2DL3$^+$ NK cells were isolated by cell sorting using antibodies against CD3 (clone S4.1; Invitrogen), CD56 (clone B159; BD), and KIR2DL2/3. This procedure typically yielded >95% CD3$^-$CD56$^+$KIR2DL3$^+$ cells.

Functional assays

Stimulatory plastic surfaces for IFN-γ secretion and degranulation assays were prepared using 96-well plates (Maxisorp; Thermo Fisher Scientific). First, a layer of SA (Prozyme) was immobilized on the surfaces followed by incubation with biotinylated anti-NKG2D antibody (α-NK, clone 1D11; Abcam) and HLA-Cw3 protein. In general, α-NK was used at 1 µg/ml, and HLA-Cw3 was used at 1 µg/ml. In cases in which one or more of these constituents was left out, a nonstimulatory biotinylated mouse MHC molecule (either I-E^k or H2-D^b) was added to bring the total protein concentration to 2 µg/ml. After protein immobilization, 2–3 × 10^5 NKL cells were added to each well, and the plate was incubated at 37°C for 30 min (for degranulation) or 16 h (for IFN-γ secretion). For degranulation experiments, we found that a 30-min incubation time in the absence of monensin or brefeldin yielded optimal responses. All functional assays were performed in the presence of 200 IU/ml IL-2. IFN-γ secretion experiments were performed in triplicate and quantified by ELISA using a mouse monoclonal antibody (clone K3.53; R&D Systems) for capture and a biotinylated affinity-purified goat IgG (R&D Systems) for detection. For degranulation experiments, 5 µg/ml phycoerythrin-Cy5–conjugated anti-CD107a antibody (clone H4A3; BD) was included at the start of the 37°C incubation. After washing, CD107a staining was quantified by flow cytometry. For the analysis shown in Fig. 1 D, the level of activation-induced degranulation was determined by subtracting the percentage of CD107a$^+$ cells in unstimulated samples. UV irradiation of HLA-Cw3(cage) was performed using a handheld UV lamp for 20 min before protein immobilization. All flow cytometric data were analyzed using FlowJo software (Tree Star, Inc.).

Flow cytometric analysis of Ca^{2+} signaling

Stimulation by antibody cross-linking was performed using α-NK, biotinylated anti-2B4 (α-2B4, clone C1.7; eBioscience), and anti-KIR2DL2 (α-KIR, clone GL183; Beckman Coulter). α-KIR was cross-linked with α-NK and α-2B4 using F(ab')$_2$ goat anti–mouse IgG (α-Mouse; Jackson Immunoresearch Laboratories, Inc.). For Ca^{2+} flux assays, 2–3 × 10^5 NKL cells were loaded with 5 µg/ml Fluo-4AM (Invitrogen) and incubated in 50 µl of complete RPMI 1640 on ice in the presence or absence of 10 µg/ml α-NK, 10 µg/ml α-2B4, and 20 µg/ml α-KIR. After ≥15 min, cells were diluted in 500 µl of warm complete RPMI 1640 and incubated at 37°C for 2 min followed immediately by flow cytometric analysis. α-NK and α-2B4 were cross-linked by the addition of 20 µg/ml SA ∼1 min after the start of the flow cytometry experiment. α-KIR was cross-linked to α-NK and α-2B4 by the addition of 20 µg/ml α-Mouse. Data were collected for a total of 10 min. Fluo-4AM loading and flow cytometry were performed in the presence of 2.5-mM probenecid (Invitrogen).

Supported lipid bilayers

A 10:1 mixture of 1,2-dioleoyl-*sn*-glycero-3-phosphocholine and biotinyl cap phosphoethanolamine (both obtained from Avanti Polar Lipids, Inc.) was resuspended in PBS and emulsified into small unilamellar vesicles using a lipid extruder (Avanti Polar Lipids, Inc.). 8-well glass-chamber slides (Thermo Fisher Scientific) were cleaned by sonication in 2% Hellmanex (Helma Analytics) at 50°C followed by extensive washing in deionized water. Small unilamellar vesicle suspensions were added to the cleaned glass surfaces and allowed to form supported bilayers followed by a 30-min incubation with 20 µg/ml SA in PBS. After further washing in PBS, a mixture of biotinylated NK receptor ligands was applied for 45 min. For experiments examining KIR2DL2-mediated inhibition, ULBP3 was used at 0.5 µg/ml, ICAM was used at 1 µg/ml, and HLA-Cw3 was used at 2 µg/ml. For experiments characterizing DAP10 clustering in response to activating stimulation alone, ULBP3 was added at 0.5 µg/ml, and ICAM was added at 2 µg/ml. For phosphotyrosine-staining experiments, ULBP3 was added at 2 µg/ml, and ICAM was added at 2 µg/ml. In cases in which one or more of these constituents was left out, a nonstimulatory biotinylated mouse MHC molecule (either I-E^k or H2-D^b) was added to keep the total protein concentration constant. After protein loading, bilayers were stored at room temperature for ≤4 h before use.

Live imaging

Before imaging, cells were transferred into RPMI 1640 supplemented with 5% FCS and lacking phenol red. To inhibit myosin II and SHP-1/2, 50-µM blebbistatin (Sigma-Aldrich) and 25-µM NSC87877 (Tocris), respectively, were added to the imaging medium. 1–2-µM latrunculin and 1-mM $MnCl_2$ (both obtained from Sigma-Aldrich) were used to disrupt actin and up-regulate integrins, respectively. Mn^{2+} treatment was performed without depleting Ca^{2+} and Mg^{2+}. Live-imaging experiments used an inverted fluorescence video microscope (IX-81; Olympus) attached to an EM charge-coupled device camera (ImagEM; Hamamatsu). 488- and 561-nm lasers (CVI Melles Griot) were used for TIRF imaging of GFP and mCherry/RFP, respectively, and a Xe lamp (DG-4; Sutter Instrument Co.) was used for epifluorescence imaging. TIRF experiments used 150 or 60× objective lenses, 1.45 NA, and Ca^{2+} imaging experiments used a 20× epifluorescence objective, 0.75 NA (all objectives were obtained from Olympus). Time-lapse recordings were made using Slidebook software (Intelligent Imaging Innovations). All live imaging was performed at 37°C.

For high-resolution (150×) imaging of receptor dynamics, images were acquired every 3 or 5 s for a total of 4 min. Photostimulation was implemented using a digital diaphragm apparatus (Mosaic; Photonic Instruments) attached to a mercury lamp (HBO; Olympus). Light from the HBO lamp was filtered through a 350/50-nm bandpass to reduce photodamage. Cells were typically photostimulated during either the 25th or the 35th interval in the time lapse using a 2-s exposure.

For lower resolution TIRF imaging of cell spreading and Ca^{2+} imaging, cells were stained with PKH26 (Sigma-Aldrich; using the manufacturer's protocol) or loaded with calcium dyes (5 µg/ml Fura-2AM or Fluo-4AM), respectively. Fluo-4 loading and imaging were performed in the presence of 2.5-mM probenecid. Images were acquired every 30 or 60 s for 20–30 min after cells had been added to the bilayer. Photostimulation, when necessary, was performed using a handheld UV lamp positioned just above the chamber slide. Cells were typically photostimulated after 5–15 min using a 2-min exposure.

Image analysis

Data analysis was performed using Slidebook, Matlab (MathWorks), Prism (GraphPad Software, Inc.), and Excel (Microsoft). To quantify cell contact area, intensity thresholding was used to define the cell boundaries for every frame or every other frame in the time lapse. Only cells that formed stable symmetric contacts before UV irradiation were used for the analysis. The quantification of actin remodeling shown in Fig. 7 was performed by calculating the mean intensity of Lifeact-RFP within a central elliptical region over the length of the time lapse. For graphical representation of area and intensity data, values were normalized using images taken before UV irradiation. Microclusters of DAP10 and KIR2DL2 were traced and counted, respectively, using Matlab scripts from D. Blair (Georgetown University, Washington, DC) and E. Dufresne (Yale, New Haven, CT) based on code from E. Weeks (Emory University, Atlanta, GA), J. Crocker (University of Pennsylvania, Philadelphia, PA), and D. Grier (New York University, New York, NY). Only particles that appeared in at least four consecutive frames were used for tracing analysis. Mean microcluster velocity was derived from particle traces using Matlab. Clusters with a mean velocity <0.03 µm/s were classified as immobile, and the rest were classified as mobile. Analysis of single-cell Ca^{2+} flux in Fluo-4–loaded cells was performed by normalizing the fluorescence intensity of each cell using the last image before the initial rise in Ca^{2+}. The ensemble mean graph shown in Fig. 2 C was computed using all cells in the imaging field. The curves shown in Fig. 10 C were calculated using only cells that bound to the surface and fluxed Ca^{2+} before UV irradiation.

Staining and imaging of fixed cells

NKL cells expressing DAP10-GFP were added to bilayers containing ULBP3 and ICAM and incubated at 37°C for 15 min before fixation with 2% paraformaldehyde. After permeabilization with Triton X-100 and blocking with bovine serum albumin, the cells were stained with 1 µg/ml antiphosphotyrosine antibody (clone 4G10; Millipore) followed by 1 µg/ml Alexa Fluor 555–conjugated F(ab')$_2$ goat anti–mouse IgG (Invitrogen). After staining, the cells were imaged by TIRF microscopy at 150× magnification. Single-cell images were divided into a central region containing 40% of the contact area and a peripheral region containing the remaining 60%. Phosphotyrosine fluorescence per unit DAP10-GFP fluorescence (F_{pY}/F_{DAP10}) was determined for both regions, and the ratio of periphery/center was calculated. The mean value of this ratio for a dataset of 20 cells was 5.0 ± 1.4.

Online supplemental material

Fig. S1 shows the chemical validation of the photocaged importin-α peptide. Fig. S2 shows a schematic diagram of a typical KIR2DL2 photostimulation experiment and some additional analyses of KIR2DL2 clustering

and cellular retraction in photostimulated cells. Fig. S3 shows that Mn^{2+} impairs KIR2DL2-induced retraction. Fig. S4 shows that the formation of DAP10 microclusters requires stimulation of NKG2D. Fig. S5 schematizes the strategy used to cross-link activating and inhibitory receptors for flow cytometry–based Ca^{2+} experiments. Videos 1 and 2 show the spreading behavior of KIR2DL2-expressing NKL cells on activating and inhibitory bilayers, respectively. Videos 3 and 4 show NKL cells expressing KIR2DL2-GFP and KIR2DL2(mut)-GFP, respectively, responding to KIR2DL2 photostimulation. Video 5 illustrates the actin remodeling that takes place in response to KIR2DL2 photostimulation. Video 6 shows the formation of DAP10 microclusters in response to NKG2D stimulation. Video 7 demonstrates how photostimulation of KIR2DL2 suppresses the formation of new DAP10 microclusters in the periphery of the contact. Online supplemental material is available at http://www.jcb.org/cgi/content/full/jcb.201009135/DC1.

We thank D. Tan and members of his laboratory for help with synthetic protocols, reagents, and equipment; G. Altan-Bonnet for assistance with Matlab; L. Lanier, P. Parham, and R. Wedlich-Soldner for constructs; B. Dupont, A. Hall, F. Giancotti, and members of their laboratories for advice; B. Driscoll for technical assistance; S.S. Yi and the Memorial Sloan-Kettering Cancer Center Microchemistry Core Facility for peptide synthesis; H. Hang, K. Pham, J. Sun, T. Muir, and A. Hall for critical reading of the manuscript; and members of the M. Huse and M.O. Li laboratories for advice and encouragement.

This study was supported by a T32 postdoctoral training grant from the National Institutes of Health (T.P. Abeyweera), the Spanish Ministry of Science and Innovation (E. Merino), the Searle Scholars Program (M. Huse), and the Cancer Research Institute (M. Huse).

Submitted: 28 September 2010
Accepted: 25 January 2011

References

Abram, C.L., and C.A. Lowell. 2009. The ins and outs of leukocyte integrin signaling. *Annu. Rev. Immunol.* 27:339–362. doi:10.1146/annurev.immunol.021908.132554

Arana, E., A. Vehlow, N.E. Harwood, E. Vigorito, R. Henderson, M. Turner, V.L. Tybulewicz, and F.D. Batista. 2008. Activation of the small GTPase Rac2 via the B cell receptor regulates B cell adhesion and immunological-synapse formation. *Immunity*. 28:88–99. doi:10.1016/j.immuni.2007.12.003

Atwal, J.K., J. Pinkston-Gosse, J. Syken, S. Stawicki, Y. Wu, C. Shatz, and M. Tessier-Lavigne. 2008. PirB is a functional receptor for myelin inhibitors of axonal regeneration. *Science*. 322:967–970. doi:10.1126/science.1161151

Barber, D.F., M. Faure, and E.O. Long. 2004. LFA-1 contributes an early signal for NK cell cytotoxicity. *J. Immunol.* 173:3653–3659.

Billadeau, D.D., K.M. Brumbaugh, C.J. Dick, R.A. Schoon, X.R. Bustelo, and P.J. Leibson. 1998. The Vav–Rac1 pathway in cytotoxic lymphocytes regulates the generation of cell-mediated killing. *J. Exp. Med.* 188:549–559. doi:10.1084/jem.188.3.549

Binstadt, B.A., K.M. Brumbaugh, C.J. Dick, A.M. Scharenberg, B.L. Williams, M. Colonna, L.L. Lanier, J.P. Kinet, R.T. Abraham, and P.J. Leibson. 1996. Sequential involvement of Lck and SHP-1 with MHC-recognizing receptors on NK cells inhibits FcR-initiated tyrosine kinase activation. *Immunity*. 5:629–638. doi:10.1016/S1074-7613(00)80276-9

Binstadt, B.A., D.D. Billadeau, D. Jevremović, B.L. Williams, N. Fang, T. Yi, G.A. Koretzky, R.T. Abraham, and P.J. Leibson. 1998. SLP-76 is a direct substrate of SHP-1 recruited to killer cell inhibitory receptors. *J. Biol. Chem.* 273:27518–27523. doi:10.1074/jbc.273.42.27518

Bléry, M., J. Delon, A. Trautmann, A. Cambiaggi, L. Olcese, R. Biassoni, L. Moretta, P. Chavrier, A. Moretta, M. Daëron, and E. Vivier. 1997. Reconstituted killer cell inhibitory receptors for major histocompatibility complex class I molecules control mast cell activation induced via immunoreceptor tyrosine-based activation motifs. *J. Biol. Chem.* 272:8989–8996. doi:10.1074/jbc.272.14.8989

Boyington, J.C., S.A. Motyka, P. Schuck, A.G. Brooks, and P.D. Sun. 2000. Crystal structure of an NK cell immunoglobulin-like receptor in complex with its class I MHC ligand. *Nature*. 405:537–543. doi:10.1038/35014520

Bruhns, P., P. Marchetti, W.H. Fridman, E. Vivier, and M. Daëron. 1999. Differential roles of N- and C-terminal immunoreceptor tyrosine-based inhibition motifs during inhibition of cell activation by killer cell inhibitory receptors. *J. Immunol.* 162:3168–3175.

Bryceson, Y.T., M.E. March, D.F. Barber, H.G. Ljunggren, and E.O. Long. 2005. Cytolytic granule polarization and degranulation controlled by different receptors in resting NK cells. *J. Exp. Med.* 202:1001–1012. doi:10.1084/jem.20051143

Bryceson, Y.T., M.E. March, H.G. Ljunggren, and E.O. Long. 2006. Synergy among receptors on resting NK cells for the activation of natural cytotoxicity and cytokine secretion. *Blood*. 107:159–166. doi:10.1182/blood-2005-04-1351

Bryceson, Y.T., H.G. Ljunggren, and E.O. Long. 2009. Minimal requirement for induction of natural cytotoxicity and intersection of activation signals by inhibitory receptors. *Blood*. 114:2657–2666.

Bunnell, S.C., V. Kapoor, R.P. Trible, W. Zhang, and L.E. Samelson. 2001. Dynamic actin polymerization drives T cell receptor-induced spreading: a role for the signal transduction adaptor LAT. *Immunity*. 14:315–329. doi:10.1016/S1074-7613(01)00112-1

Burshtyn, D.N., A.M. Scharenberg, N. Wagtmann, S. Rajagopalan, K. Berrada, T. Yi, J.P. Kinet, and E.O. Long. 1996. Recruitment of tyrosine phosphatase HCP by the killer cell inhibitor receptor. *Immunity*. 4:77–85. doi:10.1016/S1074-7613(00)80300-3

Burshtyn, D.N., J. Shin, C. Stebbins, and E.O. Long. 2000. Adhesion to target cells is disrupted by the killer cell inhibitory receptor. *Curr. Biol.* 10:777–780. doi:10.1016/S0960-9822(00)00568-6

Bustelo, X.R. 2000. Regulatory and signaling properties of the Vav family. *Mol. Cell. Biol.* 20:1461–1477. doi:10.1128/MCB.20.5.1461-1477.2000

Campi, G., R. Varma, and M.L. Dustin. 2005. Actin and agonist MHC–peptide complex–dependent T cell receptor microclusters as scaffolds for signaling. *J. Exp. Med.* 202:1031–1036. doi:10.1084/jem.20051182

Culley, F.J., M. Johnson, J.H. Evans, S. Kumar, R. Crilly, J. Casasbuenas, T. Schnyder, M. Mehrabi, M.P. Deonarain, D.S. Ushakov, et al. 2009. Natural killer cell signal integration balances synapse symmetry and migration. *PLoS Biol.* 7:e1000159. doi:10.1371/journal.pbio.1000159

Das, A., and E.O. Long. 2010. Lytic granule polarization, rather than degranulation, is the preferred target of inhibitory receptors in NK cells. *J. Immunol.* 185:4698–4704. doi:10.4049/jimmunol.1001220

Davis, D.M., I. Chiu, M. Fassett, G.B. Cohen, O. Mandelboim, and J.L. Strominger. 1999. The human natural killer cell immune synapse. *Proc. Natl. Acad. Sci. USA*. 96:15062–15067. doi:10.1073/pnas.96.26.15062

Decot, V., L. Voillard, V. Latger-Cannard, L. Aissi-Rothé, P. Perrier, J.F. Stoltz, and D. Bensoussan. 2010. Natural-killer cell amplification for adoptive leukemia relapse immunotherapy: comparison of three cytokines, IL-2, IL-15, or IL-7 and impact on NKG2D, KIR2DL1, and KIR2DL2 expression. *Exp. Hematol.* 38:351–362. doi:10.1016/j.exphem.2010.02.006

Endt, J., F.E. McCann, C.R. Almeida, D. Urlaub, R. Leung, D. Pende, D.M. Davis, and C. Watzl. 2007. Inhibitory receptor signals suppress ligation-induced recruitment of NKG2D to GM1-rich membrane domains at the human NK cell immune synapse. *J. Immunol.* 178:5606–5611.

Eriksson, M., G. Leitz, E. Fällman, O. Axner, J.C. Ryan, M.C. Nakamura, and C.L. Sentman. 1999. Inhibitory receptors alter natural killer cell interactions with target cells yet allow simultaneous killing of susceptible targets. *J. Exp. Med.* 190:1005–1012. doi:10.1084/jem.190.7.1005

Esser, M.T., D.M. Haverstick, C.L. Fuller, C.A. Gullo, and V.L. Braciale. 1998. Ca^{2+} signaling modulates cytolytic T lymphocyte effector functions. *J. Exp. Med.* 187:1057–1067. doi:10.1084/jem.187.7.1057

Faure, M., D.F. Barber, S.M. Takahashi, T. Jin, and E.O. Long. 2003. Spontaneous clustering and tyrosine phosphorylation of NK cell inhibitory receptor induced by ligand binding. *J. Immunol.* 170:6107–6114.

Galandrini, R., G. Palmieri, M. Piccoli, L. Frati, and A. Santoni. 1999. Role for the Rac1 exchange factor Vav in the signaling pathways leading to NK cell cytotoxicity. *J. Immunol.* 162:3148–3152.

Garboczi, D.N., D.T. Hung, and D.C. Wiley. 1992. HLA-A2-peptide complexes: refolding and crystallization of molecules expressed in *Escherichia coli* and complexed with single antigenic peptides. *Proc. Natl. Acad. Sci. USA*. 89:3429–3433. doi:10.1073/pnas.89.8.3429

Guerra, N., F. Michel, A. Gati, C. Gaudin, Z. Mishal, B. Escudier, O. Acuto, S. Chouaib, and A. Caignard. 2002. Engagement of the inhibitory receptor CD158a interrupts TCR signaling, preventing dynamic membrane reorganization in CTL/tumor cell interaction. *Blood*. 100:2874–2881. doi:10.1182/blood-2002-02-0643

Harwood, N.E., and F.D. Batista. 2010. Early events in B cell activation. *Annu. Rev. Immunol.* 28:185–210. doi:10.1146/annurev-immunol-030409-101216

Kaufman, D.S., R.A. Schoon, M.J. Robertson, and P.J. Leibson. 1995. Inhibition of selective signaling events in natural killer cells recognizing major histocompatibility complex class I. *Proc. Natl. Acad. Sci. USA*. 92:6484–6488. doi:10.1073/pnas.92.14.6484

Krzewski, K., X. Chen, J.S. Orange, and J.L. Strominger. 2006. Formation of a WIP-, WASp-, actin-, and myosin IIA–containing multiprotein complex in activated NK cells and its alteration by KIR inhibitory signaling. *J. Cell Biol.* 173:121–132. doi:10.1083/jcb.200509076

Lanier, L.L. 2005. NK cell recognition. *Annu. Rev. Immunol.* 23:225–274. doi:10.1146/annurev.immunol.23.021704.115526

Lewis, R.S. 2001. Calcium signaling mechanisms in T lymphocytes. *Annu. Rev. Immunol.* 19:497–521. doi:10.1146/annurev.immunol.19.1.497

Lillemeier, B.F., M.A. Mörtelmaier, M.B. Forstner, J.B. Huppa, J.T. Groves, and M.M. Davis. 2010. TCR and Lat are expressed on separate protein islands on T cell membranes and concatenate during activation. *Nat. Immunol.* 11:90–96. doi:10.1038/ni.1832

Liu, D., Y.T. Bryceson, T. Meckel, G. Vasiliver-Shamis, M.L. Dustin, and E.O. Long. 2009. Integrin-dependent organization and bidirectional vesicular traffic at cytotoxic immune synapses. *Immunity*. 31:99–109. doi:10.1016/j.immuni.2009.05.009

Long, E.O. 2008. Negative signaling by inhibitory receptors: the NK cell paradigm. *Immunol. Rev.* 224:70–84. doi:10.1111/j.1600-065X.2008.00660.x

Masilamani, M., C. Nguyen, J. Kabat, F. Borrego, and J.E. Coligan. 2006. CD94/NKG2A inhibits NK cell activation by disrupting the actin network at the immunological synapse. *J. Immunol.* 177:3590–3596.

Mossman, K.D., G. Campi, J.T. Groves, and M.L. Dustin. 2005. Altered TCR signaling from geometrically repatterned immunological synapses. *Science*. 310:1191–1193. doi:10.1126/science.1119238

Nolz, J.C., L.P. Nacusi, C.M. Segovis, R.B. Medeiros, J.S. Mitchell, Y. Shimizu, and D.D. Billadeau. 2008. The WAVE2 complex regulates T cell receptor signaling to integrins via Abl- and CrkL–C3G-mediated activation of Rap1. *J. Cell Biol.* 182:1231–1244. doi:10.1083/jcb.200801121

Olcese, L., P. Lang, F. Vély, A. Cambiaggi, D. Marguet, M. Bléry, K.L. Hippen, R. Biassoni, A. Moretta, L. Moretta, et al. 1996. Human and mouse killer-cell inhibitory receptors recruit PTP1C and PTP1D protein tyrosine phosphatases. *J. Immunol.* 156:4531–4534.

Orange, J.S., K.E. Harris, M.M. Andzelm, M.M. Valter, R.S. Geha, and J.L. Strominger. 2003. The mature activating natural killer cell immunologic synapse is formed in distinct stages. *Proc. Natl. Acad. Sci. USA*. 100:14151–14156. doi:10.1073/pnas.1835830100

Ostergaard, H.L., K.P. Kane, M.F. Mescher, and W.R. Clark. 1987. Cytotoxic T lymphocyte mediated lysis without release of serine esterase. *Nature*. 330:71–72. doi:10.1038/330071a0

Peterson, M.E., and E.O. Long. 2008. Inhibitory receptor signaling via tyrosine phosphorylation of the adaptor Crk. *Immunity*. 29:578–588. doi:10.1016/j.immuni.2008.07.014

Quann, E.J., E. Merino, T. Furuta, and M. Huse. 2009. Localized diacylglycerol drives the polarization of the microtubule-organizing center in T cells. *Nat. Immunol.* 10:627–635. doi:10.1038/ni.1734

Riedl, J., A.H. Crevenna, K. Kessenbrock, J.H. Yu, D. Neukirchen, M. Bista, F. Bradke, D. Jenne, T.A. Holak, Z. Werb, et al. 2008. Lifeact: a versatile marker to visualize F-actin. *Nat. Methods*. 5:605–607. doi:10.1038/nmeth.1220

Riteau, B., D.F. Barber, and E.O. Long. 2003. Vav1 phosphorylation is induced by β2 integrin engagement on natural killer cells upstream of actin cytoskeleton and lipid raft reorganization. *J. Exp. Med.* 198:469–474. doi:10.1084/jem.20021995

Robertson, M.J., K.J. Cochran, C. Cameron, J.M. Le, R. Tantravahi, and J. Ritz. 1996. Characterization of a cell line, NKL, derived from an aggressive human natural killer cell leukemia. *Exp. Hematol.* 24:406–415.

Small, J.V., and G.P. Resch. 2005. The comings and goings of actin: coupling protrusion and retraction in cell motility. *Curr. Opin. Cell Biol.* 17:517–523. doi:10.1016/j.ceb.2005.08.004

Stebbins, C.C., C. Watzl, D.D. Billadeau, P.J. Leibson, D.N. Burshtyn, and E.O. Long. 2003. Vav1 dephosphorylation by the tyrosine phosphatase SHP-1 as a mechanism for inhibition of cellular cytotoxicity. *Mol. Cell. Biol.* 23:6291–6299. doi:10.1128/MCB.23.17.6291-6299.2003

Stinchcombe, J.C., and G.M. Griffiths. 2007. Secretory mechanisms in cell-mediated cytotoxicity. *Annu. Rev. Cell Dev. Biol.* 23:495–517. doi:10.1146/annurev.cellbio.23.090506.123521

Swat, W., and K. Fujikawa. 2005. The Vav family: at the crossroads of signaling pathways. *Immunol. Res.* 32:259–265. doi:10.1385/IR:32:1-3:259

Takayama, H., and M.V. Sitkovsky. 1987. Antigen receptor-regulated exocytosis in cytotoxic T lymphocytes. *J. Exp. Med.* 166:725–743. doi:10.1084/jem.166.3.725

Treanor, B., P.M. Lanigan, S. Kumar, C. Dunsby, I. Munro, E. Auksorius, F.J. Culley, M.A. Purbhoo, D. Phillips, M.A. Neil, et al. 2006. Microclusters of inhibitory killer immunoglobulin–like receptor signaling at natural killer cell immunological synapses. *J. Cell Biol.* 174:153–161. doi:10.1083/jcb.200601108

Valiante, N.M., J.H. Phillips, L.L. Lanier, and P. Parham. 1996. Killer cell inhibitory receptor recognition of human leukocyte antigen (HLA) class I blocks formation of a pp36/PLC-γ signaling complex in human natural killer (NK) cells. *J. Exp. Med.* 184:2243–2250. doi:10.1084/jem.184.6.2243

Varma, R., G. Campi, T. Yokosuka, T. Saito, and M.L. Dustin. 2006. T cell receptor-proximal signals are sustained in peripheral microclusters and terminated in the central supramolecular activation cluster. *Immunity*. 25:117–127. doi:10.1016/j.immuni.2006.04.010

Veldhuyzen, W.F., Q. Nguyen, G. McMaster, and D.S. Lawrence. 2003. A light-activated probe of intracellular protein kinase activity. *J. Am. Chem. Soc.* 125:13358–13359. doi:10.1021/ja037801x

Vyas, Y.M., K.M. Mehta, M. Morgan, H. Maniar, L. Butros, S. Jung, J.K. Burkhardt, and B. Dupont. 2001. Spatial organization of signal transduction molecules in the NK cell immune synapses during MHC class I-regulated noncytolytic and cytolytic interactions. *J. Immunol.* 167:4358–4367.

Vyas, Y.M., H. Maniar, C.E. Lyddane, M. Sadelain, and B. Dupont. 2004. Ligand binding to inhibitory killer cell Ig-like receptors induce colocalization with Src homology domain 2-containing protein tyrosine phosphatase 1 and interruption of ongoing activation signals. *J. Immunol.* 173:1571–1578.

Watzl, C., and E.O. Long. 2003. Natural killer cell inhibitory receptors block actin cytoskeleton-dependent recruitment of 2B4 (CD244) to lipid rafts. *J. Exp. Med.* 197:77–85. doi:10.1084/jem.20020427

Yokosuka, T., and T. Saito. 2010. The immunological synapse, TCR microclusters, and T cell activation. *Curr. Top. Microbiol. Immunol.* 340:81–107. doi:10.1007/978-3-642-03858-7_5

Yokosuka, T., K. Sakata-Sogawa, W. Kobayashi, M. Hiroshima, A. Hashimoto-Tane, M. Tokunaga, M.L. Dustin, and T. Saito. 2005. Newly generated T cell receptor microclusters initiate and sustain T cell activation by recruitment of Zap70 and SLP-76. *Nat. Immunol.* 6:1253–1262. doi:10.1038/ni1272